Abdominal Radiology
https://doi.org/10.1007/s00261-023-03877-2

REVIEW

Infarcts and ischemia in the abdomen: an imaging perspective with an emphasis on cross-sectional imaging findings

Ali Devrim Karaosmanoglu[1] · Omer Onder[1] · Volkan Kizilgoz[2] · Peter F. Hahn[3] · Mecit Kantarci[2,4] · Mustafa Nasuh Ozmen[1] · Musturay Karcaaltincaba[1] · Deniz Akata[1]

Received: 13 January 2023 / Revised: 23 February 2023 / Accepted: 24 February 2023

Abstract

Infarcts and ischemia of abdominal organs may present with acute abdominal pain, and early diagnosis is crucial to prevent morbidity and mortality. Unfortunately, some of these patients present in poor clinical conditions to the emergency department, and imaging specialists are crucial for optimal outcomes. Although the radiological diagnosis of abdominal infarcts is often straightforward, it is vital to use the appropriate imaging modalities and correct imaging techniques for their detection. Additionally, some non-infarct-related abdominal pathologies may mimic infarcts, cause diagnostic confusion, and result in delayed diagnosis or misdiagnosis. In this article, we aimed to outline the general imaging approach, present cross-sectional imaging findings of infarcts and ischemia in several abdominal organs, including but not limited to, liver, spleen, kidneys, adrenals, omentum, and intestinal segments with relevant vascular anatomy, discuss possible differential diagnoses and emphasize important clinical/radiological clues that may assist radiologists in the diagnostic process.

Graphical abstract

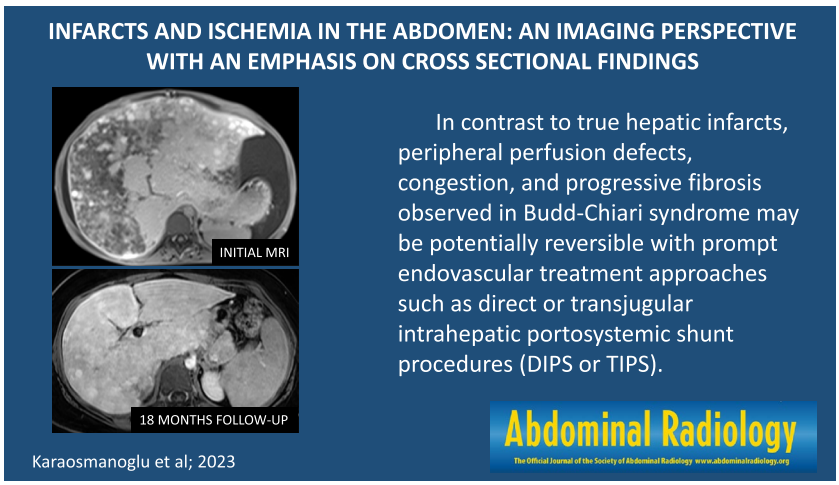

Keywords Infarction · Abdomen · CT · MR · Cross-sectional imaging

Abbreviations

HI	Hepatic infarction
HA	Hepatic artery
PV	Portal vein
T1W	T1-weighted
T2W	T2-weighted
BCS	Budd–Chiari syndrome
BN	Biliary necrosis
AIDS	Acquired immunodeficiency syndrome
MRCP	Magnetic resonance cholangiopancreatography
PTC	Percutaneous transhepatic cholangiography

✉ Ali Devrim Karaosmanoglu
alidevrim76@yahoo.com

Extended author information available on the last page of the article

Published online: 18 March 2023

PSC	Primary sclerosing cholangitis
AMI	Acute mesenteric ischemia
BI	Bowel infarction
SMA	Superior mesenteric artery
CTA	CT angiography
VMI	Veno-occlusive mesenteric ischemia
RI	Renal infarction
RCN	Renal cortical necrosis
SI	Splenic infarction
AI	Adrenal infarction
IV	Intravenous
DIC	Disseminated intravascular coagulation
DWI	Diffusion-weighted imaging
AOI	Acute omental infarcts
AEA	Acute epiploic appendagitis
APA	Acute perigastric appendagitis
OT	Ovarian torsion
STI	Segmental testicular infarction

Introduction

Infarcts in the abdominal organs could be common and may cause clinical diagnostic confusion. The symptoms are mostly nonspecific, and acute onset abdominal pain, sometimes localized, is the most common presenting symptom. Abdominal organ infarcts may be self-limiting with supportive treatment or can be catastrophic in some clinical situations. Therefore early diagnosis is critical for optimal clinical management, and imaging plays an essential role in properly triaging patients.

In this article, we aimed to outline the general imaging approach, present cross-sectional imaging findings of abdominal ischemia and infarcts with an organ-based approach, discuss possible differential diagnoses, and emphasize important clinical/radiological clues that may assist radiologists in the diagnostic process. An organ-based comprehensive summary of infarcts and ischemia in the abdomen can be found in Tables 1 and 2.

General imaging approach

US findings are generally nonspecific, and US has limited diagnostic utility except for a few organs such as the testis and ovary. Doppler US, on the other hand, is an operator-dependent examination but might be useful as it allows non-invasive evaluation of the relevant vascular anatomy and parenchymal resistive index in real-time and portable conditions. It can be used as an important gatekeeper in identifying critically ill patients and directing them to contrast-enhanced cross-sectional imaging, if necessary.

CT (and more rarely MRI) with intravenous contrast is the primary diagnostic tool for diagnosing and managing infarcts. CT appears to be the workhorse modality with its high speed and wide availability in emergency departments. However, MRI can be a good alternative on a case-by-case basis due to its superior soft tissue resolution and the absence of ionizing radiation.

Infarcts and ischemia in solid abdominal organs and hollow viscera may present with different imaging findings, and should be handled differently in terms of cross-sectional imaging.

In solid abdominal organs such as the liver, spleen, and kidney, infarcts are generally observed as triangular or wedge-shaped peripheral lesions or hypoenhancing geographical areas. Standard postcontrast portal venous phase images are very useful in showing the affected area. Again in this phase, it is possible to evaluate the presence of complications such as superposed infection, to follow infarct progression, and to evaluate the patency of major visceral veins. Additional arterial phase images are essential for detecting major arterial occlusion, especially in the patient group thought to benefit from endovascular treatment or revascularization surgery. However, it is not always possible to distinguish abdominal infarcts from non-infarct-related pathologies. In these equivocal cases, dynamic contrast-enhanced cross-sectional imaging combined with the subtraction technique can be a problem-solver. After subtraction, at least some enhancement is observed in masses, which is not expected in infarcts.

On the other hand, acute bowel ischemia is an entity that can progress rapidly to infarction, has a mortal course, and sometimes presents with very subtle findings. In the presence of clinical suspicion, it is critical to demonstrate vascular patency in the arterial and venous phases after intravenous contrast administration. Additionally, when bowel ischemia is suspected, the use of neutral oral contrast, such as water, is recommended instead of positive oral contrast. Because positive oral contrast may hinder the evaluation of vascular anatomy by distorting maximum-intensity projection images, and may make the detection of early stage enhancement changes in the bowel wall challenging [1]. Last but not least, current literature indicates that dual-energy CT applications can facilitate the detection of small bowel ischemia. Thanks to the increased conspicuity via iodine mapping, enhancement changes in the bowel wall can be detected at an earlier stage, visualization of the entire mesenteric vasculature can be improved despite single-phase imaging, the presence of intramural hematoma can be demonstrated with virtual non-contrast images, and all these advantages can be achieved using a much lower dose of intravenous contrast agent [2, 3].

Table 1 Organ-based comprehensive summary of infarcts and ischemia in the abdomen (part-1)

Disease	Imaging findings	Auxiliary clinical information
Hepatic infarct	Peripherally located wedge-shaped hypoenhancing area. Hypointense on T1W and hyperintense on T2W images. Extensive infarction may present with hypoenhancing areas with geographic distribution	History of possible iatrogenic reasons, including surgery, ablation, endovascular procedures, and transplantation may be suggestive. Should also be considered in the presence of other underlying causes such as trauma, vasculitis, HELLP syndrome, and severe shock
Biliary necrosis	Strictures and dilatations in the intrahepatic bile ducts, multiple bilomas, peribiliary necrotic tissues, and intraductal filling defects representing debris or sludge may be seen. Hepatic artery thrombosis is generally the underlying condition	History of vasculitis, systemic infections, cardioembolic episodes, trauma, liver transplantation, or transcatheter chemoembolization may be helpful. Progressively increasing bilirubin levels despite all necessary biliary interventions may be suggestive
Arterial occlusive mesenteric ischemia	Endoarterial thrombus/filling defect. Paper-thin bowel wall. Air densities within the bowel wall, mesenteric fat planes and/or mesenteric venous branches. Air–fluid levels within dilated bowel loops may also be seen	Advanced age. Severe atherosclerotic disease or cardioembolic conditions. Severe abdominal pain disproportionate to physical examination findings may be suggestive
Veno-occlusive mesenteric ischemia	Endovenous thrombus/filling defect. Mesenteric congestion and fat stranding, intraabdominal free fluid, abnormal thickening of segmental bowel loops with target appearance. In advanced stages, bowel perforation may be seen	May present with acute-onset progressive diffuse colicky pain, abdominal distension, and blood in the stool. Presence of possible underlying causes, including hypercoagulable state, recent surgery, and systemic infections may be helpful
Renal infarct	Pyramidal or wedge-shaped hypoenhancing areas mostly without any significant mass effect. «Cortical rim sign» may be observed in cases of global renal infarction. «Reverse rim sign» is typical of renal cortical necrosis	Patients may present with flank pain, nausea, vomiting, and fever. Presence of possible underlying causes, including infective endocarditis, atrial fibrillation, advanced atherosclerosis, surgical or endovascular interventions, rheumatological and hematological diseases may be helpful
Splenic infarct	Pyramidal or wedge-shaped hypoenhancing area. In the subacute and chronic phases, involution of the infarcted parenchyma with cystic transformation may be seen. In case of global infarction, splenic capsular enhancement may be observed. Splenic infarcts generally appear hypointense compared to the normal spleen parenchyma on both T1W and T2W images	Variable symptomatology ranging from asymptomatic presentation to severe left upper quadrant pain. Presence of possible underlying causes, including hemoglobinopathies, cardioembolism, lymphoproliferative diseases, certain infections (infectious mononucleosis, malaria), rheumatological conditions, pancreatitis, and splenic torsion may be helpful

Table 2 Organ-based comprehensive summary of infarcts and ischemia in the abdomen (part-2)

Disease	Imaging findings	Auxiliary clinical information
Non-hemorrhagic adrenal infarct	Non-enhancing, slightly thickened adrenal glands. Enhancing thin rim surrounding the infarcted parenchyma may be seen. Diffuse parenchymal hyperintensity on T2W images and parenchymal restricted diffusion on DWI may be other suggestive findings	Rare. Generally secondary to pregnancy, antiphospholipid antibody syndrome, hereditary thrombophilias, or conditions that may cause extensive micro-arteriolar thrombi such as DIC. Patients may present with abdominal pain, nausea, vomiting, and even acute adrenal crisis
Hemorrhagic adrenal infarct	Glandular enlargement secondary to diffuse macroscopic adrenal hemorrhage, which appears as hyperdense on non-enhanced CT and hyperintense on T1W pre-contrast MR images	Same as non-hemorrhagic adrenal infarcts
Intraperitoneal focal fat infarction	*Omental necrosis* triangular-shaped large heterogeneous fatty mass in the omentum *Epiploic appendagitis* oval-shaped fat-containing lesion (< 5 cm) surrounded by inflammatory fat stranding located at the antimesenteric border of the colon. «Central dot sign» may be seen *Perigastric appendagitis* oval-shaped, heterogeneous lesion located in the falciform, gastrohepatic, or gastrosplenic ligaments and accompanied by peripheral fat stranding	Self-limiting conditions with non-specific clinical presentation, which may mimic other more serious causes of acute abdominal pain. Patients generally present with well-localized, non-migrating, relatively constant abdominal pain. Nausea, vomiting, anorexia, and fever may also accompany the pain. Heavy food intake, local trauma, rapid body movement, and coughing may trigger IFFI
Ovarian torsion	Enlarged and displaced ovary, heterogeneous ovarian stroma due to edema and hemorrhage, peripherally displaced follicles, pelvic free fluid, and «twisted pedicle sign». Other suggestive findings include the absence of parenchymal enhancement on MRI and lack of internal vascularity on Doppler US. T2 hypointense ovarian rim may also be seen	Should be considered in female patients with acute pelvic pain. Early diagnosis and intervention are crucial to prevent irreversible tissue loss. Previous history of ovarian torsion/detorsion episodes may be a clue
Testicular torsion	Testicular enlargement, change in the echotexture, and twisting of the spermatic cord on gray scale US. Decreased, absent, or abnormally high-resistance flow in the symptomatic testis on Doppler US	One of the most common reasons of acute scrotum. Early diagnosis and intervention are crucial to prevent irreversible tissue loss
Segmental testicular infarct	Wedge-shaped heterogeneous lesion with the apex pointing to the testicular mediastinum on scrotal US. Absent flow within the lesion on Doppler US Non-enhancing, relatively well-defined heterogeneous parenchymal area peripherally outlined by capsular rim enhancement on post-contrast MR images	Rare. Acute scrotal pain. Presence of possible underlying causes including vasculitis, trauma, hematological diseases, and epididymo-orchitis

Liver infarction

Hepatic infarction (HI) is rare due to the dual blood supply of the liver from the hepatic artery (HA) and the portal vein (PV). The presence of extensive collaterals is another contributing factor to the rarity of HI. Despite being the main feeding vessel of the liver, PV occlusion rarely causes HI, per se [4]. HI occurs commonly in patients with HA occlusion or PV thrombosis with concomitant HA occlusion [4].

In modern medical practice, HI related to iatrogenic reasons are also common. Surgery [5], percutaneous ablation [6], endovascular tumor treatments [7], transjugular intrahepatic portosystemic shunt procedure [8], and liver transplantation [9] may be counted among the iatrogenic causes. Systemic vasculitis, trauma, infection, severe shock, preeclampsia or HELLP (hemolytic anemia, elevated liver enzymes, low platelets) syndrome, and hypercoagulability are the other rarer reasons for HI [10, 11].

On imaging, HI typically is seen on CT as a wedge-shaped hypoenhancing area with its base abutting on the liver capsule and its apex pointing towards the liver hilum. The infarcted areas appear as hypointense areas on T1-weighted (T1W) images and hyperintense on T2-weighted (T2W) images (Fig. 1). Geographic distribution may also be observed in patients with larger infarcts (Fig. 2).

Abscess formation may be seen in the infarcted areas due to the secondary infection. During follow-up imaging, intralesional gas formation, rounding of the lesion contours, and development of an enhancing wall are considered as red flags suggesting superinfected infarction [12]. However, the differential diagnosis between the sterile infarcts and abscesses using imaging findings solely is not always possible, and in case of suspicion, percutaneous sampling is needed (Fig. 3).

Despite the fact that diagnosing hepatic parenchymal infarcts is generally straightforward, caution should be exercised to differentiate parenchymal infarcts from focal fatty infiltration, abscess, or neoplastic processes (Fig. 4) [13, 14]. In-phase/opposed-phase imaging can be used to assess the presence of fat infiltration in areas that appear hypodense on contrast-enhanced CT. Dynamic contrast-enhanced MR imaging can show contrast-enhancing areas of neoplastic lesions and enhancing walls of abscesses. Diffusion-weighted imaging (DWI) can provide additional information by revealing restricted diffusion caused by the purulent content within the abscess cavity or hypercellular regions of neoplastic lesions.

Apart from those above-mentioned well-known entities, hepatic perfusion disorders and pseudoinfarcts (Zahn's infarcts, infarct-like cyanotic atrophy) should

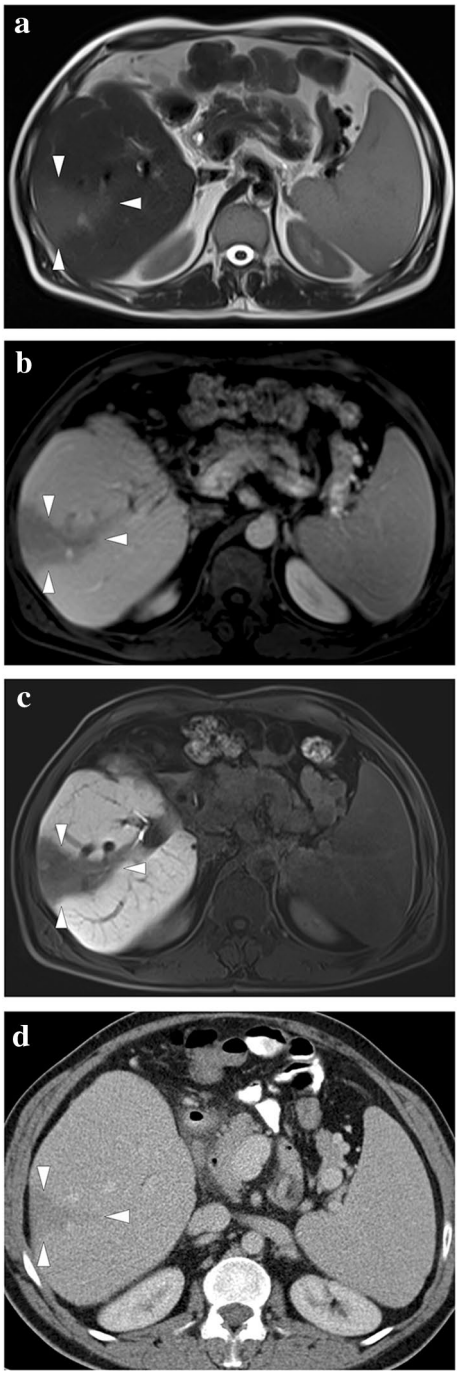

Fig. 1 A 44-year-old male patient with a history of liver transplantation due to HBV-related cirrhosis now presenting with right upper quadrant pain and elevated LFTs. **a** Axial plane T2-weighted MR image showed a triangular-shaped mildly hyperintense lesion adjacent to the capsule (arrowheads). **b** Axial plane T1-weighted postcontrast image demonstrated peripherally located, wedge-shaped hypoenhancing parenchymal area (arrowheads). **c** Hepatobiliary phase MR image with hepatospecific contrast agent clearly demonstrated this abnormal parenchymal area (arrowheads). Clinical symptomatology and imaging findings were thought to represent hepatic infarction. **d** Follow-up CT image 6 months after the initial MR examination demonstrated regression of the non-enhancing parenchyma in the infarcted segment (arrowheads)

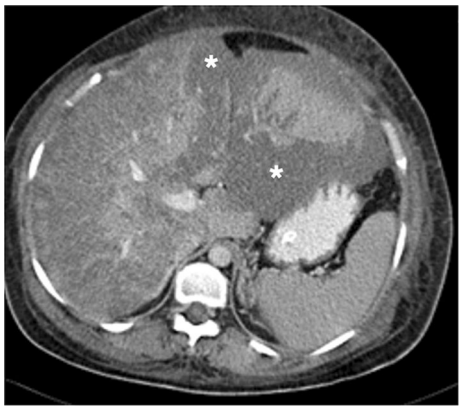

Fig. 2 A 37-year-old female patient with 34 weeks of pregnancy presented with malaise, severe right upper quadrant pain, lethargy, significantly elevated LFTs, thrombocytopenia, and hemolytic anemia. The clinical and laboratory findings highly suggested HELLP syndrome, and an emergency cesarean section (C/S) was performed. The patient's lethargy and abdominal pain progressed, and emergent abdominal and cranial CT scans were performed 2 days after the delivery. Axial plane postcontrast abdominal CT image showed extensive liver infarction as hypodense areas with geographic distribution (asterisks). Her head CT was within normal limits (not shown). The patient responded well to ICU care and was discharged without apparent clinical sequela 1 month after the CT scan

be considered in the differential diagnosis of true HI. Although pseudoinfarcts can only be confirmed in the histopathological examination, they should be considered, especially in cases of hepatic and portal venous occlusion [10, 15]. PV occlusion or PV branch stenosis generally presents with early arterial enhancement in the affected parenchyma due to arterial buffer response or arterioportal shunting, and parenchymal homogenization is expected in the portal venous phase [16]. On the other hand, impaired hepatic venous outflow initially causes centrilobular congestion, and subsequent parenchymal atrophy develops due to the chronically elevated intrasinusoidal pressure [17, 18]. Unlike true HI, congestion and atrophy predominance with no apparent coagulation necrosis is expected histologically in pseudoinfarcts [15]. In the acute phase of Budd–Chiari syndrome (BCS), pseudoinfarcts may be observed as peripheral hypoattenuating parenchymal areas on CT. This finding may be related to parenchymal congestion, edema, and steatosis (Fig. 5) [17, 19]. In addition, the so-called "straight border sign" may be seen in these cases and refers to the linear demarcation border between the normal and hypoperfused portions of the liver parenchyma (Fig. 6) [20]. Radiologists should be aware that in contrast to true HI, peripheral perfusion defects, congestion, and progressive fibrosis observed in BCS may be potentially reversible with prompt endovascular treatment approaches such as direct or transjugular intrahepatic portosystemic shunt procedures (Fig. 7) [19].

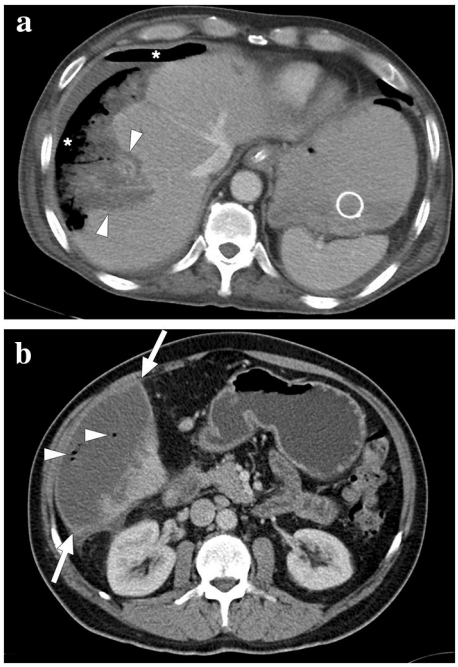

Fig. 3 Two different patients with complicated liver infarcts. **a** A 65-year-old male patient with pancreatic adenocarcinoma underwent a Whipple operation. Three weeks after the operation, the patient presented with severe hematemesis. CT angiography revealed a gastroduodenal artery pseudoaneurysm as the underlying cause of upper gastrointestinal tract bleeding (not shown). An emergent catheter angiography and subsequent percutaneous embolization were performed. Ten days after the embolization, the patient again presented to ER with high fever, hypotension, and severe right upper quadrant pain. Axial plane postcontrast CT image showed necrotic liver parenchyma (arrowheads) with subcapsular and subdiaphragmatic air densities (asterisks). The constellation of imaging findings was found to represent the superinfection of the gangrenous liver segment. Emergent surgery was planned, but the patient expired 3 h after the CT scan. **b** A 57-year-old male patient underwent catheter angiography embolization of the giant liver hemangioma in segment 6. Twelve days after the embolization, the patient presented to the ER with a high fever, chills, and right upper quadrant pain. An emergent contrast-enhanced abdominal CT showed a large infarcted area in segment 6 (arrows) with air bubbles within this parenchymal segment (arrowheads). The imaging and clinical findings were considered to represent a superinfection of the infarcted parenchyma. Imaging-guided aspiration revealed purulent content and confirmed the diagnosis

Biliary ischemia and necrosis

Biliary necrosis (BN), also known as ischemic cholangiopathy, is an entity characterized by focal or extensive damage to the intrahepatic bile duct epithelium secondary to the impaired blood supply to these structures. The bile ducts are predominantly supplied by the peribiliary plexus originating from the HA, unlike the dual supply of hepatocytes, and any interruption of flow from these small arterioles may cause necrosis of the biliary epithelium [21].

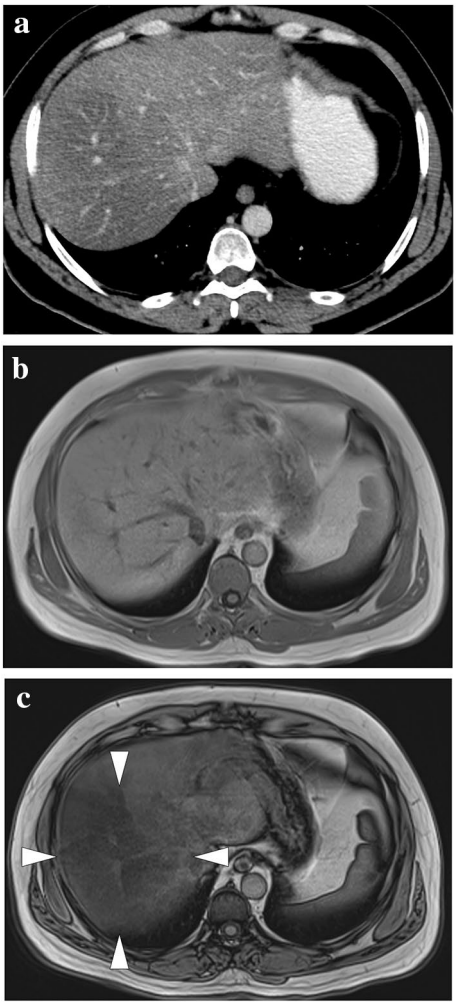

Fig. 4 A 44-year-old male patient with known squamous cell carcinoma of the tongue. **a** Axial plane postcontrast abdominal CT showed a large hypodense area within the right liver lobe with a relatively sharp demarcation line from the remaining parenchyma (arrowheads). **b** and **c** In (**b**) and out (**c**) of phase MR images confirmed the presence of focal hepatic steatosis (arrowheads)

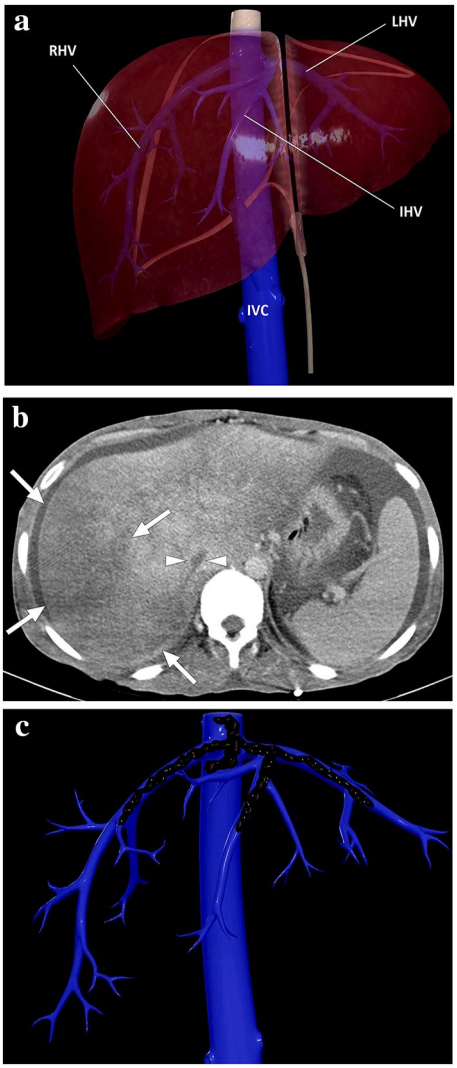

Fig. 5 **a** A 3D illustration shows normal hepatic venous anatomy. *IVC* inferior vena cava, *RHV* right hepatic vein, *IHV* intermediate hepatic vein, *LHV* left hepatic vein. **b** A 25-year-old male patient with longstanding Behcet's disease presented to ER with acute onset diffuse abdominal pain, predominantly in the right upper quadrant. Physical examination revealed a tender and enlarged liver. Axial plane postcontrast CT image demonstrated thrombosed inferior vena cava (arrowheads) and all three hepatic veins. Clinical and imaging findings were compatible with Budd–Chiari syndrome. Heterogeneously enhancing liver was seen with prominent enhancement in the central parts compared to the peripheral parenchyma. The hypoattenuating area in the peripheral portion of the right liver lobe was thought to be consistent with a parenchymal pseudoinfarct representing congestion and edema (arrows). **c** 3D illustration image represents the distribution of the thrombi in the hepatic veins and vena cava inferior, consistent with Budd–Chiari syndrome

Several diseases may cause HA thrombosis and BN. Vasculitic (such as polyarteritis nodosa), infectious (AIDS), cardioembolic, traumatic, or iatrogenic (liver transplantation or transarterial chemoembolization) processes may all result in BN [21]. Additionally, Osler–Weber–Rendu disease may lead to chronic biliary ischemia due to the stealing of blood from the biliary tree secondary to extensive hepatic arteriovenous shunting and may present with irregular biliary dilatation in the liver [22]. As the imaging findings may all look similar in all these different entities, clinical history is critical in these patients.

CT and MRCP are both frequently used non-invasive imaging modalities in these patients. Beading appearance secondary to the alternating strictures and dilatations in the intrahepatic bile ducts, multiple bilomas, and peribiliary necrotic tissues may be counted among the typical imaging findings [23]. Air bubbles and air–fluid levels may be observed within bilomas/necrotic collections, and this finding does not always indicate the presence of a concomitant infection (Fig. 8). Because pneumobilia is a normal finding

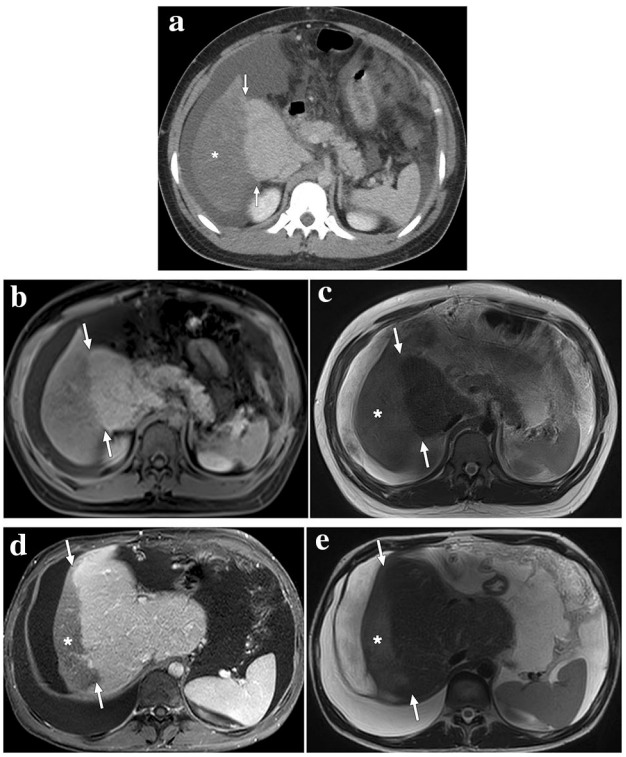

Fig. 6 A 20-year-old male patient with no significant medical history presented with acute abdominal distention and elevated liver enzymes. **a** Axial plane postcontrast abdominal CT showed widespread thrombi in the hepatic veins, which was found to be consistent with Budd–Chiari syndrome (not shown). «Straight border sign» (arrows) is seen as a sharp demarcation line between the enhancing central and hypoenhancing peripheral liver parenchyma (asterisk). **b** Same sharp demarcation (arrows) could also be clearly observed in the post-contrast T1W axial plane image. **c** Peripheral hypoperfused parenchyma had high signal intensity on T2-weighted images (asterisk) and was considered to represent a hepatic pseudoinfarct. The patient was treated conservatively with anticoagulation and repeated paracentesis. **d** and **e** Follow-up abdominal MRI obtained 6 months after the initial episode revealed atrophy of the previously involved peripheral hypoenhancing parenchyma (asterisks) and enlarged central zone with preserved demarcation line (arrows)

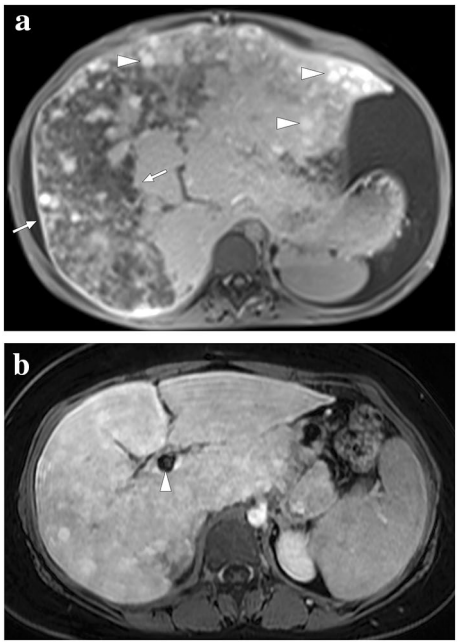

Fig. 7 A 19-year-old female patient with known Budd–Chiari syndrome secondary to essential thrombocytosis. **a** Axial plane postcontrast MR image showed peripheral hypoperfused parenchyma within the right liver lobe (arrows). Also noted were ascites and multiple regenerative parenchymal nodules (arrowheads). The patient subsequently underwent a direct intrahepatic portocaval shunt procedure. **b** Contrast-enhanced MRI 18 months after the initial presentation showed almost complete homogenization of the liver parenchyma and disappearance of ascites. Note was also made of the intrahepatic portocaval shunt (arrowhead)

in patients who have had a biliary intervention and biliary air may communicate with the collection. Therefore, air–fluid levels can be observed within sterile bilomas [23]. Color Doppler US is a practical imaging test for evaluating the patency of the HA in patients with liver transplants. Also, spectral Doppler US can be used to diagnose HA stenosis, which may cause post-transplant biliary complications. Tardus-parvus wave-form, decreased hepatic resistive index (<0.5), and prolonged systolic acceleration time are diagnostic for HA stenosis [23].

Interventional radiology plays a critical role in diagnosing and managing complications related to HA occlusion in patients with liver transplants, including BN. Percutaneous transhepatic cholangiography (PTC) may particularly reveal dilation of bile ducts and leakage of contrast medium into the periportal space [23]. In the presence of chronic ischemic changes, intraductal filling defects may represent endoluminal debris or sludge (Fig. 9). In rare cases, the gallbladder may also be affected due to the BN, and linear endoluminal filling defects secondary to the sloughed gallbladder epithelium may be observed [23].

Caroli's disease, periportal edema, peribiliary cysts, and primary sclerosing cholangitis (PSC) may all be considered in the differential diagnosis [23]. In Caroli's disease, saccular dilatation of the intrahepatic bile ducts may mimic bilomas. However, the «central dot sign», which represents malformed biliary cysts encircling the portal radicle, is very helpful in differential diagnosis on CT. Periportal edema is expected to occur on both sides of the portal triads, whereas intrahepatic bile duct dilatation is usually unilateral. Peribiliary cysts are generally observed in the setting of chronic liver disease or autosomal dominant polycystic kidney disease. Although they rarely cause diagnostic confusion due to intrahepatic bile duct dilatation via mass effect, peribiliary cysts generally do not pose any diagnostic difficulties. On the other hand, PSC may pose a particular diagnostic challenge on cholangiographic examinations. However, intrahepatic peribiliary

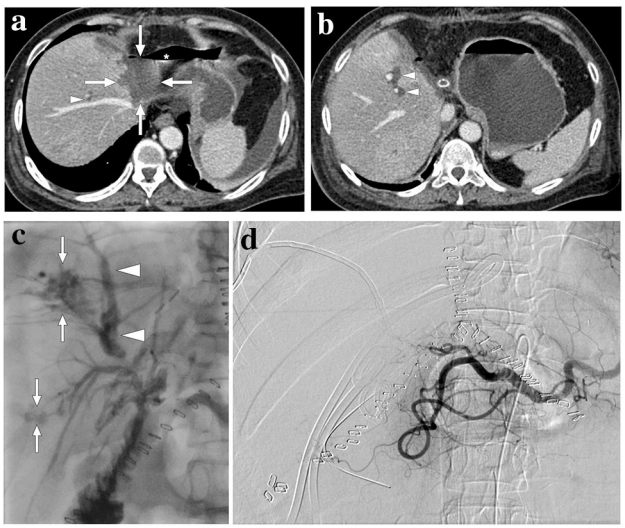

Fig. 8 A 55-year-old female patient with a 2-year history of primary sclerosing cholangitis underwent right liver lobe transplantation from a living donor. On day 4 after the transplantation surgery, the abdominopelvic CT exam was within normal limits (not shown). On day 10, bile containing serous fluid leakage was observed through the abdominal incision scar. **a** and **b** Axial plane postcontrast abdominal CT images showed a newly developed collection (arrows) containing air–fluid levels (asterisk) along the resection line between the liver and stomach, which was found to represent a biloma. Mild dilatation in the intrahepatic bile ducts was also observed (arrowheads). Subsequent percutaneous transhepatic cholangiography (PTC) demonstrated leakage from the biliary anastomosis site, and percutaneous biliary drainage was subsequently performed. During follow-up, serum bilirubin levels increased progressively despite adequate biliary drainage. **c** Three months after the transplantation, follow-up PTC revealed dilatation of intrahepatic bile ducts (arrowheads) and leakage of contrast medium into the periportal space (arrows). **d** To rule out ischemic cholangiopathy, invasive angiography was performed, which revealed the complete occlusion of the hepatic artery. Unfortunately, the patient's clinical condition deteriorated progressively, and the patient expired due to biliary sepsis 2 weeks after the angiography

collections or bilomas are not among the frequent imaging findings of PSC [23].

Bowel ischemia and infarction

Acute mesenteric ischemia (AMI) may progress to bowel infarction (BI) in a significant percentage of patients. Despite the improvements in diagnosis and treatment, the mortality rate is still high, around 50–60% [24]. Early diagnosis and treatment may significantly improve clinical outcomes, so prompt diagnosis is crucial. In patients with delayed treatment, more than 24 h, the mortality rate approaches 100% [25]. Most patients present at advanced ages, and the mortality rate increases significantly with advancing age [26, 27]. BI may be related to mesenteric arterial and venous causes. Embolic and thrombotic diseases of the mesenteric arteries are common reasons for BI, but mesenteric venous thrombosis should also be considered in the differential diagnosis.

Arterial embolism to the superior mesenteric artery (SMA) is the most common cause of AMI, representing 40–50% of the cases [28]. The heart is the most common embolic source in these patients. Therefore, atrial fibrillation, myocardial infarction, and ventricular aneurysm should be sought after in these patients. Its acute take-off from the abdominal aorta makes this vessel especially vulnerable to emboli which typically lodge 6–8 cm beyond the SMA origin. Arterial thrombosis is another important cause of AMI, representing 25% of the cases, and atherosclerosis is the most common predisposing factor in these patients. Patients with SMA thrombosis secondary to atherosclerosis are generally expected to have pre-existing symptoms of chronic mesenteric ischemia, such as weight loss, "food fear", or postprandial pain. Also, unlike embolism, occlusion usually develops at the SMA origin in cases with SMA thrombosis. Less common non-atherosclerotic causes of SMA thrombosis include SMA dissection, vasculitis involvement, or mycotic aneurysms [29].

Non-occlusive mesenteric ischemia is a poorly understood entity. Severe vasospasm is thought to be the underlying etiology. This entity is associated with systemic diseases, such as shock, severe sepsis, myocardial infarction, and renal and hepatic diseases [30].

Irreversible ischemia and subsequent transmural BI typically occur within 6 h in subjects with complete luminal occlusion [31]. Initially, patients may present with severe abdominal pain disproportionate to physical examination findings. The infarction of the muscular layer and the neural elements, adynamic ileus, and luminal distension occur with progression to transmural infarction. At this stage, bowel perforation and peritonitis occur with subsequent death.

As stated above, imaging plays a fundamental role in the diagnosis as the clinical findings may be nonspecific. Abdominal CT, coupled with CT angiography (CTA), is typically the imaging modality of choice due to its high temporal and spatial resolution, as well as wide availability. CT is beneficial in this clinical situation as it can pinpoint the culprit abnormalities in the mesenteric vessels. It may also help diagnose (or rule out) the other acute intraabdominal conditions that may clinically mimic AMI and BI. Triphasic CT with non-contrast images followed by arterial and venous phase images allows evaluation of vascular atherosclerosis as well as arterial and venous luminal patency with high sensitivity. Arterial and venous phases also allow evaluation of the end organ findings and the bowel walls.

The embolus in the SMA is seen as a filling defect in the arterial phase. The exact location of the emboli and the extent of the endoluminal thrombus are identified in this phase. Reformatted images in different planes may help orient the clinicians (Fig. 10). A paper-thin bowel wall may

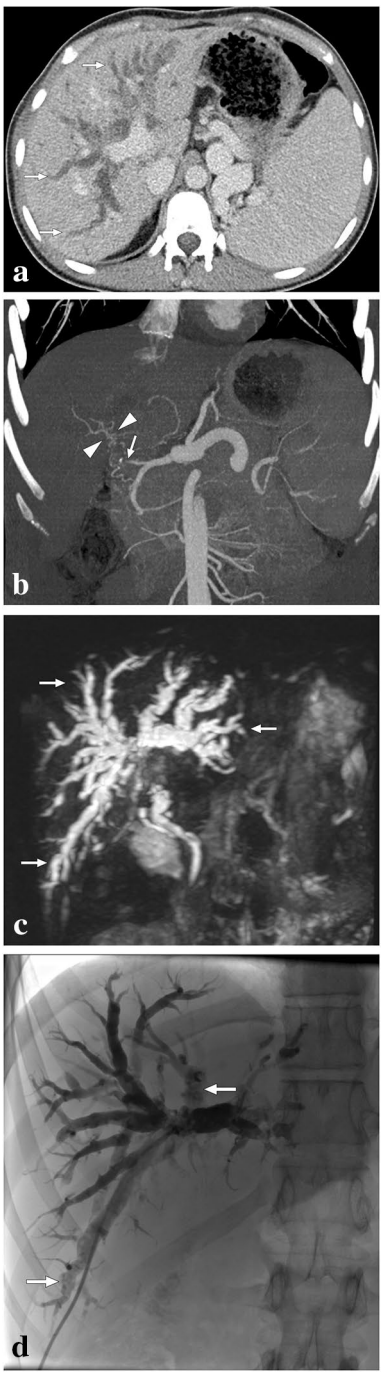

Fig. 9 A 20-year-old male who had undergone cadaveric whole liver transplantation due to autoimmune hepatitis presented with new-onset jaundice 10 months after the transplantation. Hepatobiliary US showed diffuse dilatation of intrahepatic bile ducts, and spectral Doppler US revealed a low hepatic arterial resistive index. **a** Axial plane postcontrast CT image demonstrated extensive intrahepatic bile duct dilation (arrows). Also noted were splenomegaly and enlarged splenic veins. **b** CT Angiography showed total occlusion of the hepatic artery graft (arrow) with multiple small-sized arterial collaterals (arrowheads) at the level of the hepatic hilus. **c** 3D-MRCP image better demonstrated the extent of biliary involvement, which may also suggest an obstructive biliary dilatation secondary to a hepatic hilar mass. The constellation of imaging findings suggested ischemic cholangiopathy, and the patient was managed conservatively with repeated biliary drainage interventions. **d** PTC image 2 years after the transplantation showed biliary sludge and debris formation (arrows) within the dilated intrahepatic bile ducts, and biliary drainage revealed purulent bile content. Despite repeated biliary interventions and appropriate medical treatment, the patient's hepatic functions gradually deteriorated, and a re-transplantation was planned. Unfortunately, the patient expired before the second liver transplantation

indicate the loss of intestinal muscle tone and transmural infarction. The detection of air within the bowel wall and within the lumens of the mesenteric venous branches and the PV are other important indicators of transmural BI (Fig. 11).

Veno-occlusive mesenteric ischemia (VMI) is a less common cause of AMI and generally develops secondary to superior mesenteric vein thrombosis. It may present with acute-onset, progressively worsening diffuse colicky abdominal pain. Abdominal distension and the presence of blood in the stool may also be seen. In the later stages, VMI may lead to mortality by causing the development of bowel necrosis, perforation, and sepsis. The underlying causes of VMI include a hypercoagulable state, portal hypertension, recent intraabdominal surgery, and intraabdominal infections. On CT, a filling defect in a mesenteric vein, mesenteric fat stranding, intraabdominal free fluid, and abnormal thickening of the bowel loops with target appearance can be seen in patients with VMI (Fig. 12). The extent of bowel involvement mainly depends on the location of thrombi as occlusion of small-sized segmentary venous branches presents with much more localized bowel edema (Fig. 13).

Other clinical entities presenting with segmental and symmetrical bowel wall thickening, such as inflammatory bowel disease, infections, radiation enteritis, spontaneous intramural bowel hematoma, portal enteropathy, and angioedema should all be considered in the differential diagnosis of VMI [32]. A detailed evaluation of the clinical history is usually helpful in differentiating these various diseases (Fig. 14). After excluding the endovenous thrombus with CT angiography, differential diagnosis can be narrowed in accordance with other accompanying imaging findings and patient history.

Surgery and endovascular interventions are the two fundamental therapeutic approaches for bowel ischemia. Surgical resection of the ischemic/infarcted bowel segments and surgical thromboembolectomy are two basic approaches in surgery. In addition, a second-look laparotomy within 48 h after the first surgery to assess the viability of the bowel wall may be necessary for certain patients [24].

Endovascular techniques are increasingly used in the treatment of AMI. This approach is typically used in the early stages of the disease before the peritoneal findings and imaging findings of transmural BI appear. Endovascular

Fig. 10 A 92-year-old female patient with known atrial fibrillation presented to ER with acute severe abdominal pain. Physical examination findings were disproportionate to the severity of her symptoms and showed a soft and non-tender abdomen. Abdominal CT Angiography was ordered to rule out mesenteric vascular disease. Sagittal-oblique reformatted CT angiography image showed superior mesenteric artery (SMA) occlusion secondary to an embolus lodging approximately 8 cm distal to the SMA origin (arrows). Emergency surgery with intestinal resection and thrombectomy was performed

approaches seem to be extremely promising when patients are appropriately selected [33].

Renal infarction

Renal infarction (RI) is an uncommon clinical condition, and therefore, the index of suspicion is low. It is one of the rare causes of acute abdominal pain, and its clinical diagnosis is difficult [34]. Flank and/or abdominal pain are the common presenting symptoms. Nausea, vomiting, and fever are not common at the time of initial diagnosis [35]. RI should be especially considered in patients with known atrial fibrillation or bacterial endocarditis who present with flank pain. Advanced atherosclerosis, medical renal diseases, dehydration, fibromuscular dysplasia, sickle cell disease, rheumatologic diseases, and iatrogenic conditions (related to endoarterial catheter interventions) are other predisposing factors [34]. Arterial causes are the most common reason for RI, whereas, albeit rare, venous causes may also cause parenchymal infarcts in the kidney. Traumatic complete or partial devascularization of the kidney should also be considered in trauma cases having flank pain (Fig. 15). In these trauma patients, it is thought that the intimal injury within the wall of the renal artery induces luminal thrombosis, which causes subsequent RI [36].

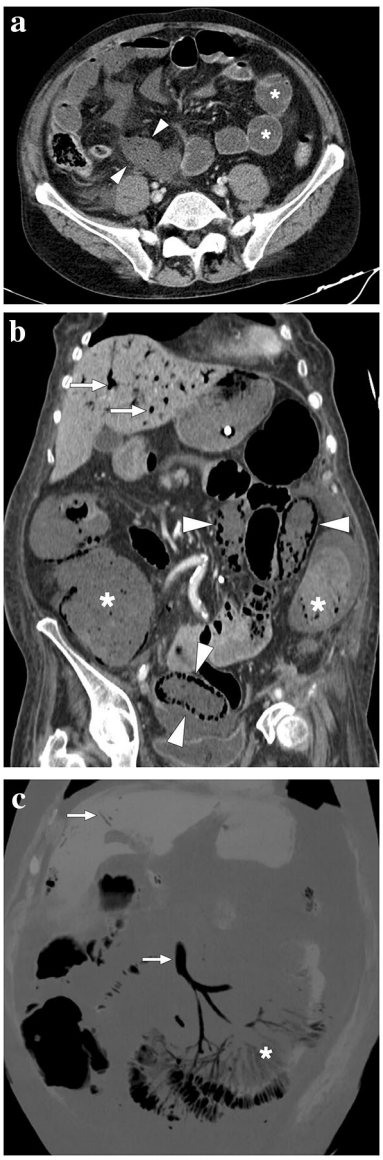

Fig. 11 **a** A 59-year-old male patient with known metastatic gastric cancer presented with signs and symptoms of shock. Axial plane postcontrast CT images showed multiple dilated small bowel loops (asterisks) with no sign of abrupt transition point suggestive of mechanical obstruction. In addition, there were some small bowel segments with no appreciable wall (arrowheads) suggestive of mural necrosis. Emergent surgery confirmed long-segment small bowel necrosis. **b** A 77-year-old female patient with a history of colon cancer presented to ER with findings suggestive of metabolic shock. Coronal plane postcontrast abdominal CT image showed dilated bowel loops (asterisks), widespread pneumatosis intestinalis (arrowheads), and air bubbles within intrahepatic portal vein branches (arrows). Imaging findings were found to be suggestive of extensive transmural intestinal infarction. Surgery confirmed almost complete necrosis of the small bowel segments. **c** A 62-year-old male patient presented with acute kidney injury, diffuse abdominal pain, and hypotension. Non-enhanced abdominal CT showed pneumatosis intestinalis, air densities within the mesenteric veins, and intrahepatic portal vein branches suggestive of transmural bowel necrosis. Coronal plane minimum-intensity projection CT image better demonstrated the air within distal mesenteric veins (asterisk). Also noted were air densities within the superior mesenteric vein and intrahepatic portal vein branches (arrows). Surgery confirmed intestinal necrosis

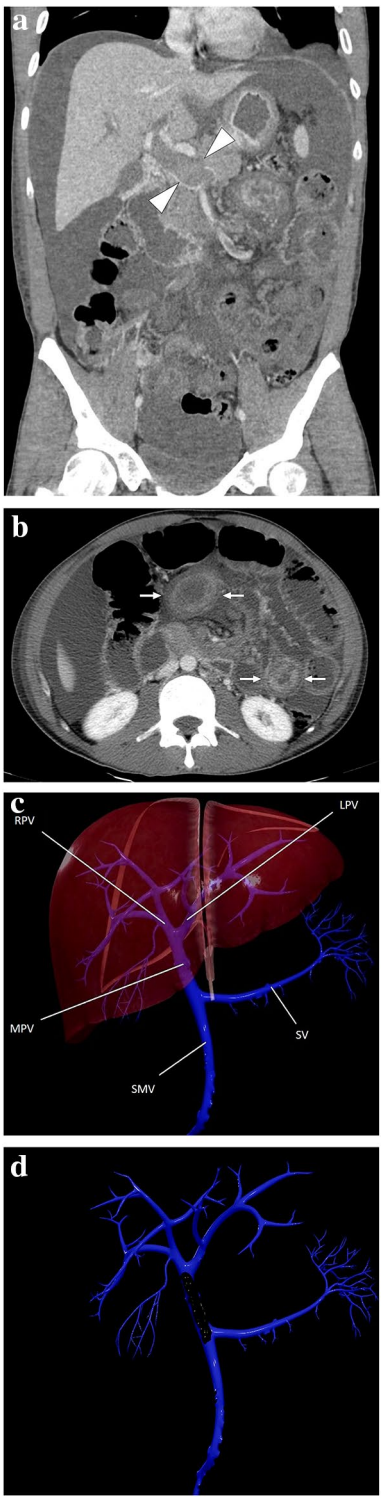

Fig. 12 A 33-year-old male patient with an unremarkable past medical history presented to the ER with diffuse abdominal pain and progressive abdominal distention. **a** Coronal plane postcontrast abdominal CT image showed a large bland thrombus obliterating the main portal vein (arrowheads), edematous small bowel loops, and diffuse ascites. **b** Axial plane image of the same CT study better demonstrated target-like wall thickening of the small bowels (arrows). Imaging findings were found to be consistent with veno-occlusive mesenteric ischemia. Emergent surgery confirmed imaging findings. Hematological work-up after surgery diagnosed factor V Leiden mutation-associated thrombophilia. **c** 3D illustration of portal vein branches (*SV* splenic vein, *SMV* superior mesenteric vein, *MPV* main portal vein, *RHPV* right portal vein, *LHPV* left portal vein) and **d** the representation of the thrombus lying along the main portal vein ▶

Abdominal CT, with associated CTA, studies are the most commonly used cross-sectional imaging modalities for evaluating RI. Wedge-shaped parenchymal hypoenhancing areas without significant mass effect are the typical imaging findings of a focal parenchymal infarct. However, the mass effect may be observed in infarcted areas in certain patients, and these areas may be confused with a space-occupying neoplasm. MRI, with subtraction images, may be helpful in these patients to rule out an underlying neoplastic process by proving the absence of contrast enhancement, which suggests parenchymal infarction (Fig. 16).

RI may give rise to the "cortical rim sign", which refers to devascularization of the affected renal parenchyma with only thin cortical enhancement. This sign, seen in approximately 50% of renal infarcts, is secondary to preserved collateral capsular perfusion. In case of branch occlusion of the renal artery, the renal capsular artery, an early branch of the renal artery, may not be affected. Thanks to the perforating branches of the renal capsular artery, rim-shaped enhancement can be seen in the renal capsule and subcapsular area [37].

Apart from hypoenhancing infiltrative neoplasms, pyelonephritis, and renal contusion are the other main differential diagnoses of RI. Although not entirely distinctive, pyelonephritis should always be considered in patients with clinical signs of infection, elevated serum inflammatory markers, and other ancillary imaging findings that may suggest inflammation. Unlike RI, the "cortical rim sign" is not typically observed in patients with pyelonephritis [38]. Focal parenchymal renal contusion should also be considered in patients with trauma. Contusions are generally observed as ill-defined, round, or ovoid-shaped hypoattenuating areas, in contrast to sharply demarcated and wedge-shaped infarcts [39].

Renal allograft infarction is a rare but serious complication of renal transplant surgery [40]. Parenchymal infarcts in these patients may appear in global or segmental fashions. Accompanying cortical rim sign may also be seen and could be helpful as a diagnostic clue (Fig. 17). Allograft infarcts mainly develop in the early postoperative period and occur secondary to the main branch or segmental renal artery thromboses. The most common causes of this clinical phenomenon include hyperacute rejection, renal artery kinking, and anastomotic occlusion [40]. Color and spectral Doppler US are both beneficial for early diagnosis. Segmental allograft

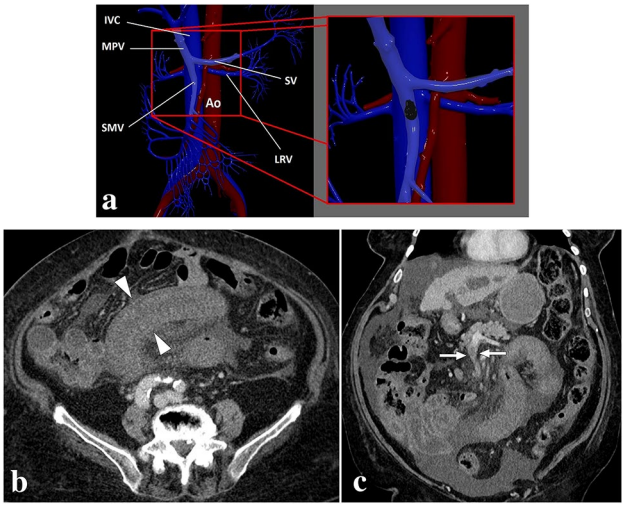

Fig. 13 **a** 3D illustration of SMV and its branches for a quick review. The magnified view represents a thrombus in the main SMV branch (*IVC* inferior vena cava, *HPV* hepatic portal vein, *SV* splenic vein, *Ao* abdominal aorta, *SMV* superior mesenteric vein, *LRV* left renal vein). **b** An 83-year-old male patient with known hepatocellular carcinoma presented with acute onset diffuse abdominal pain. Axial plane postcontrast CT showed symmetrical wall thickening in a long segment of small bowel loops (arrowheads) accompanied by mesenteric fat stranding. **c** Coronal plane CT image demonstrated thrombosed mesenteric segmental vein (arrows) draining the affected small bowel loops. Imaging findings were consistent with segmental veno-occlusive mesenteric ischemia, and the patient was treated accordingly

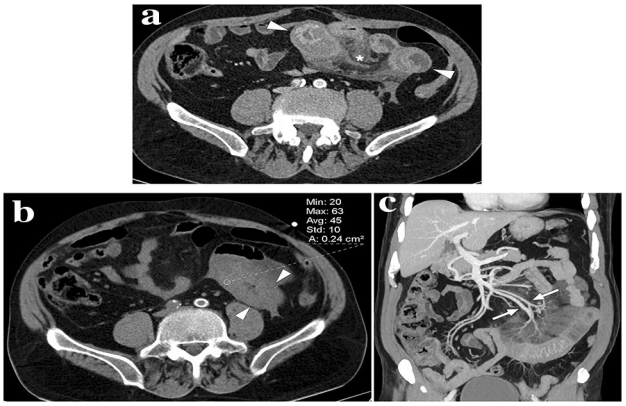

Fig. 14 A 68-year-old male patient presented with abdominal pain in the left lower quadrant. The patient was on chronic coumadin use due to prior mitral valve replacement surgery. **a** Axial plane postcontrast abdominal CT showed diffuse wall thickening in a long segment of distal ileal loops with accompanying mesenteric fat stranding (asterisk) and minimal pelvic free fluid of high density suggesting hemorrhagic nature (not shown). **b** Axial plane non-enhanced abdominal CT image revealed that the thickened intestinal wall segments have a density of 45 HU, suggesting hemorrhage. It would not be possible to distinguish between bowel wall enhancement versus hemorrhage with only venous phase CT images. **c** Coronal plane reformatted maximum intensity projection image confirmed the patency of mesenteric arterial/venous structures (arrows) related to the involved bowel segment. Clinical presentation and radiological findings were found to be consistent with spontaneous intestinal intramural hematoma. The INR was found to be significantly elevated after the CT study. The patient responded well to supportive treatment

infarcts can be observed as an avascular hypoechoic ill-defined mass on color Doppler US and may closely mimic focal pyelonephritis [40]. Correlation with the clinical and laboratory findings may be helpful for correct diagnosis in patients with equivocal imaging findings. Cross-sectional or invasive angiography should be liberally used in these patients to diagnose renal artery occlusion at an early stage.

Renal cortical necrosis (RCN) should also be considered in the presence of hypoenhancing kidneys. The pathological hallmark of RCN is the detection of fibrin thrombi in the renal capillaries. The pathogenesis of RCN is not well described and appears to be multifactorial. Reduced arterial blood flow due to vasospasm, sepsis, postpartum hemorrhage, and shock seems to be the primary abnormality leading to RCN [41]. The disease is more common in neonates and early postpartum females [42]. Contrast-enhanced CT is the most commonly used imaging modality for diagnosis. Nonenhancing and hypoattenuating cortical rim with simultaneous enhancement of the renal medulla is the typical imaging finding, also called the "reverse rim sign" (Fig. 18). The constellation of imaging findings correlates with the histopathologic features of the disease [43–45].

Splenic infarction

Spleen is a highly vascular solid organ, and the distal branches of the splenic artery are noncommunicating end arteries. This anatomic structure leads to parenchymal infarcts in the spleen when these distal branches occlude. Splenic infarction (SI) can be due to iatrogenic and non-iatrogenic reasons.

Non-iatrogenic splenic infarcts

Among the causes of non-iatrogenic SI are: infections such as infectious mononucleosis and malaria, hemoglobinopathies (sickle cell anemia being a common reason), cardiac emboli, lymphoproliferative disorders, collagen vascular diseases, pancreatitis, portal hypertension, and splenic torsion (Fig. 19) [46, 47].

Clinical symptomatology is highly variable in these patients. Splenic infarcts can be clinically silent or severely symptomatic with acute left upper quadrant pain. The size and distribution of the infarct areas are variable, from focal small-area infarcts to complete SI. Parenchymal abscesses, pseudocyst formations, splenic rupture, and hemorrhage are among the potential complications of SIs [48, 49].

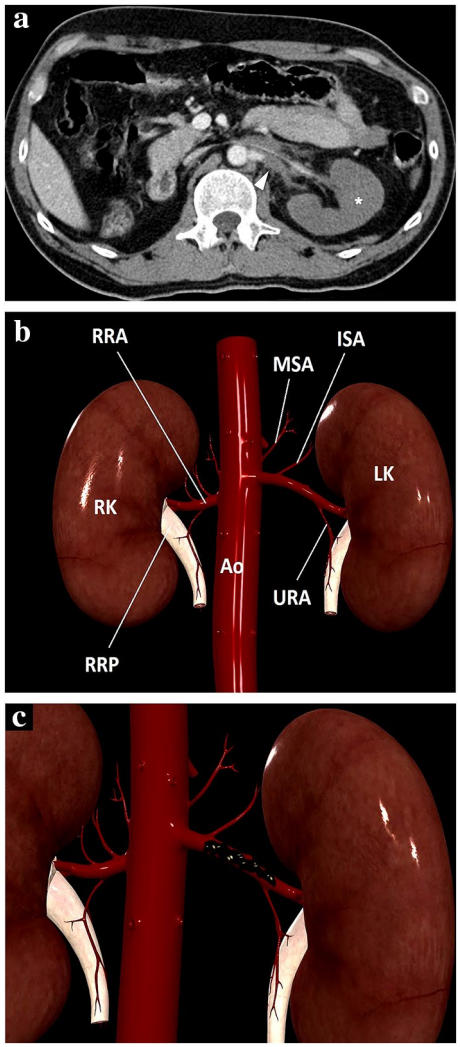

Fig. 15 **a** A 39-year-old male patient with a known left solitary kidney was brought to the ER after high-energy trauma. Axial plane post-contrast abdominal CT image showed a thrombosed left renal artery (arrowhead) and complete devascularization of the left renal parenchyma with no apparent parenchymal enhancement (asterisk). An arterial graft was surgically placed between the abdominal aorta and left renal hilus to establish renal vascularization. **b** 3D illustration indicates renal arteries and some important major branches for a quick review. *MSA* middle suprarenal artery, *ISA* inferior suprarenal artery, *URA* ureteric branches of the renal artery, *Ao* Abdominal aorta, *RRA* right renal artery, *RK* right kidney, *LK* left kidney, *RRP* right renal pelvis. **c** Representation of thrombus in the lumen of the left renal artery

On US, the SIs present as ill-defined, wedge-shaped, or nodular hypoechoic areas, but US has limited sensitivity and was found to be diagnostic in only 18% of the patients [50].

CT is the workhorse imaging modality for diagnosing SI due to its high sensitivity. On contrast-enhanced CT, SIs appear as wedge-shaped, hypoattenuating areas demonstrating poor enhancement in the acute period after infarction occurs. As the process advances to the subacute phase, the

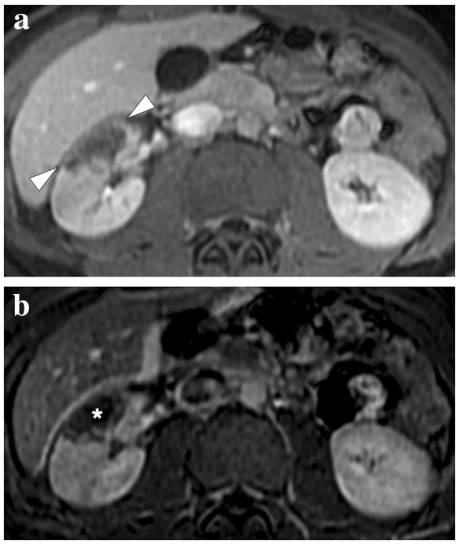

Fig. 16 A 19-year-old male patient with known hereditary thrombophilia presented with recent onset right flank pain. An initial US examination was unremarkable except for mild heterogeneity, without any obvious mass lesion, in the interpolar region of the right kidney (not shown). **a** Axial plane T1-weighted dynamic postcontrast abdominal MR image showed a triangular-shaped hypointense, nonenhancing area (arrowheads) in the right kidney, which was found to be suggestive of renal infarction. **b** Axial plane subtraction image confirmed the absence of focal contrast enhancement (asterisk)

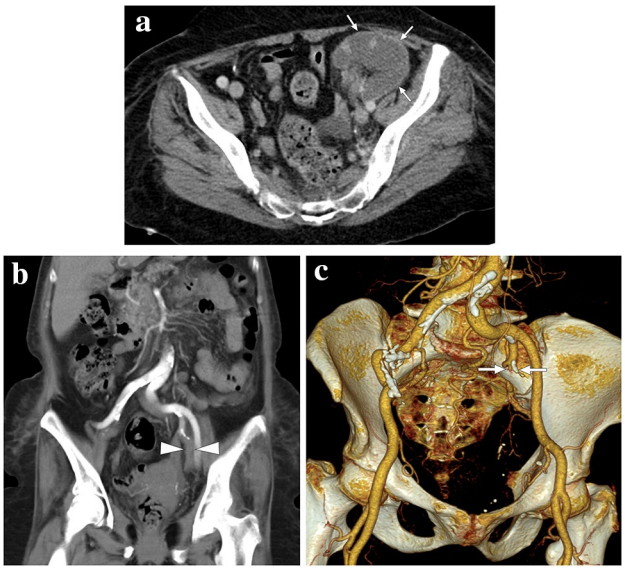

Fig. 17 A 65-year-old female with a history of renal transplantation nearly 20 years ago presented with severe, acute left lower quadrant pain. **a** Axial plane postcontrast CT showed complete devascularization of graft kidney with cortical rim sign (arrows). **b** and **c** Coronal plane reformatted CT angiography (**b**) and 3D-VRT images (**c**), respectively, demonstrated the acute thrombotic occlusion (arrowheads) and the remaining stump of the renal artery (arrows) anastomosed to the left internal iliac artery

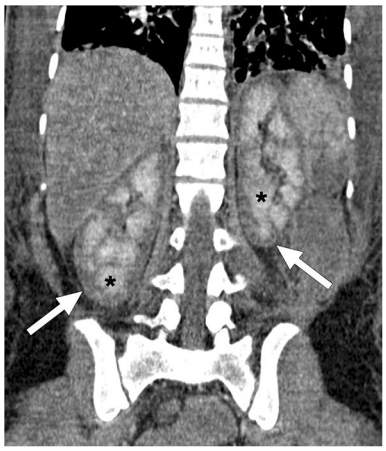

Fig. 18 A 25-year-old female patient developed disseminated intravascular coagulation and multi-organ failure secondary to the amniotic fluid embolism after a complicated C/S. Coronal plane postcontrast abdominal CT image showed hypoenhancing renal cortices (arrows) with accompanying medullary enhancement (asterisks), the so-called reverse rim sign, in bilateral kidneys. Imaging findings were found to be consistent with renal cortical necrosis

infarcted area may appear cystic with the involution of the dead parenchyma in the chronic phase (Fig. 20). The demarcation line between the infarcted and non-infarcted areas may be more prominent in the subacute phase [46]. The liquefaction and expansion of the infarcted area on follow-up imaging are alarming findings for superimposed infection, and these imaging findings appear more commonly in SIs caused by thromboembolism. Image-guided aspiration and sampling may be considered for managing these patients [46]. Global SI may occur when the splenic artery becomes completely thrombosed due to thrombus formation or tumor invasion. In these patients, the only enhancing area of the spleen may be the splenic capsule demonstrating rim enhancement (Fig. 21) [51].

MRI is rarely used for the initial diagnosis of SI. The decreased parenchymal signal on both T1W and T2W images is thought to be secondary to fibrosis, calcification, and hemosiderin deposition [52]. The demarcation line of preserved and infarcted parenchyma may be better outlined on MRI with dynamic post-contrast T1W imaging.

As a differential of non-iatrogenic SI, acute splenic sequestration crisis should be considered in patients with sickle cell anemia if the massive enlargement of the spleen is seen with capsular rim sign and global absence of parenchymal enhancement. Although it is quite rare in the adult population, recognition of this condition, which causes hypersplenism secondary to blood pooling in the spleen due to entrapment of sickled erythrocytes in the microvascular bed, could be critical for patient management. Because splenic sequestration increases the risk of splenic rupture, and splenectomy may be required. In these cases,

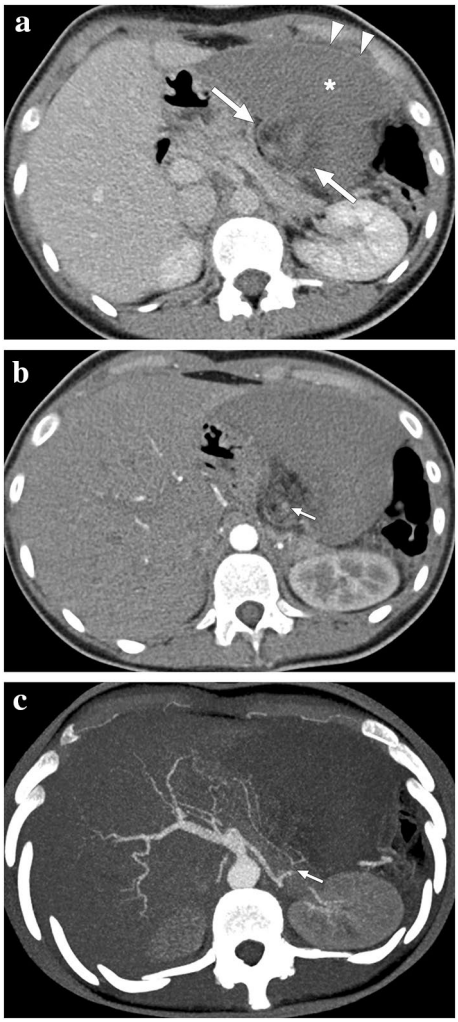

Fig. 19 A 17-year-old female patient presented to ER with abdominal pain. Abnormal position and anteromedial displacement of the spleen were noted on abdominal US (not shown). **a** Axial plane postcontrast abdominal CT showed global absence of contrast enhancement in the spleen parenchyma (asterisk), capsular rim enhancement (arrowheads), and «whirl sign» in the splenic pedicle (arrows). **b** Axial plane arterial phase image demonstrated a relative lack of enhancement in the splenic artery at the splenic pedicle (arrow). **c** Axial plane arterial phase maximum intensity projection image better demonstrated the focal cut-off in the twisted splenic artery (arrow). Imaging findings were compatible with global splenic infarction due to splenic torsion. Emergency laparotomy was performed, and histopathological examination of the torsed spleen revealed extensive coagulation necrosis with severe congestion

the splenic artery and vein are expected to be patent in the contrast-enhanced examination as opposed to the typical SI. However, it has been reported that the contrast filling in the splenic vein is counterintuitively retrograde from the PV. Lack of flow void and luminal hyperintensity due to the slow flow in the splenic vessels on T2W imaging might be helpful in making the diagnosis (Fig. 22) [47].

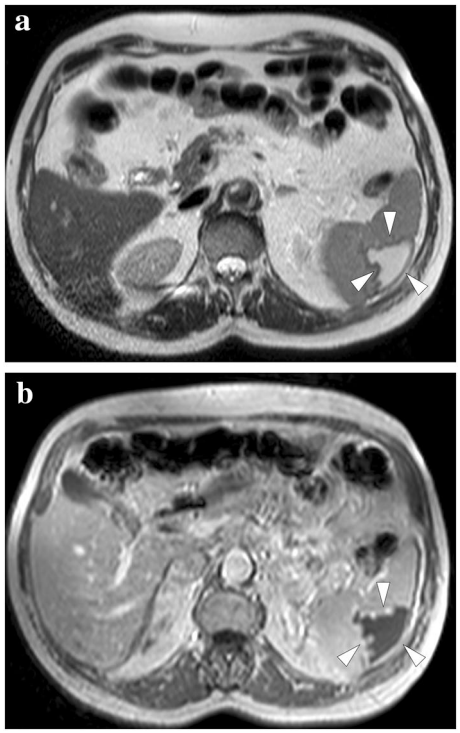

Fig. 20 A 63-year-old male with previously diagnosed splenic infarction due to atrial fibrillation in an outside institution. **a** and **b** Axial plane T2 and post-contrast T1-weighted MR images, respectively, showed peripherally located, triangular-shaped, well-demarcated, T2-hyperintense, and T1-hypointense nonenhancing parenchymal area (arrowheads). These findings were found to represent cystic-liquefying changes in the subacute phase

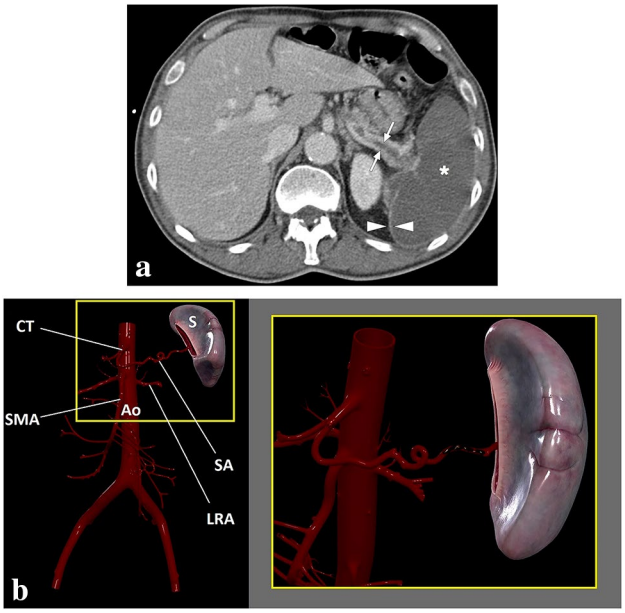

Fig. 21 A 68-year-old male patient with known lung cancer and polycythemia vera presented with acute onset severe left upper quadrant pain. **a** Axial plane postcontrast abdominal CT showed thrombosed splenic artery (arrows) and global splenic infarction (asterisk). Also, note was made of enhancing splenic capsule (arrowheads). **b** 3D illustration shows the splenic artery and some major branches of the abdominal aorta (*S* spleen, *CT* celiac trunk, *Ao* abdominal aorta, *SMA* superior mesenteric artery, *LRA* left renal artery, *SA* splenic artery). The magnified view demonstrates the thrombosis of the splenic artery

Iatrogenic splenic infarcts

Iatrogenic SIs can occur as complications of various surgical procedures such as hemicolectomy, nephrectomy, and a variety of endovascular interventions for embolization or bleeding control, or they can be induced intentionally and therapeutically in patients with hypersplenism [53–55]. As expected, the management of iatrogenic SIs secondary to the procedural adverse events differs from those induced therapeutically since the latter does not present any initial diagnostic challenge and may require follow-up imaging for the treatment response.

Emerging as a viable alternative to surgery in patients with hypersplenism, minimally invasive endovascular splenic embolization was initially performed to embolize the whole splenic parenchyma. However, this approach has largely been abandoned in modern practice due to several severe complications associated with the procedure, such as abscess formation, splenic rupture, and life-threatening sepsis. To mitigate the complications of this procedure, partial splenic embolization, paired with antibiotic and vaccine prophylaxis, gained popularity due to its better outcomes and favorable complication rates. Abdominal CT and US may be performed pre-procedurally to establish the splenic volume and the patency of the splenoportomesenteric venous axis [56].

Follow-up CT is typically performed 1 week after the procedure to assess the percentage of infarcted tissue. Immediate post-procedure CT is not typically performed, but the threshold for ordering a CT should be low in patients with immediate hypotension and fever to rule out splenic rupture or abscess (Fig. 23). CT is beneficial to evaluate the success of the procedure. On CT, a sharp demarcation line between the infarcted and viable splenic parenchyma is easily visible on post-contrast images. In the months following the procedure, the spleen size gradually decreases, as expected (Fig. 24). Follow-up imaging may not be necessary at this phase, and most patients are monitored clinically [56].

Adrenal infarction

Adrenal infarction (AI) is a rare but serious condition that usually presents with nonspecific symptoms such as abdominal pain, nausea, and vomiting. It is well-known that pregnancy, antiphospholipid antibody syndrome, and

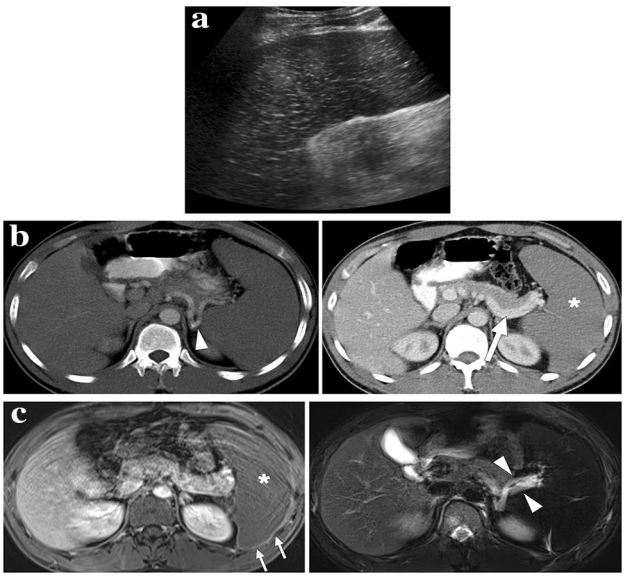

Fig. 22 A 26-year-old male with known sickle cell-beta thalassemia trait presented to ER with left upper quadrant pain. **a** Longitudinal-oblique gray scale US image showed an enlarged spleen with diffuse parenchymal hypoechogenicity and multiple hyperechoic foci scattered throughout the parenchyma. **b** and **c** Axial plane arterial (**b**) and venous (**c**) phase CT images demonstrated the patency of the splenic artery (arrowhead, **b**) and splenic vein (arrow, **C**). However, diffuse hypoenhancement of the spleen was noted on the venous phase CT image (asterisk, **c**). **d** and **e** Axial plane T1-weighted postcontrast (**d**) and T2-weighted fat-suppressed (**e**) images showed absent parenchymal enhancement (asterisk, **d**), capsular rim enhancement (arrows, **d**) and hyperintense splenic vessels at the hilus due to slow flow (arrowheads, **e**). Diffuse splenic hypointensity secondary to iron deposition was also noted on axial T2-weighted image (**e**). Clinical and radiological findings were found to be compatible with acute splenic sequestration crisis. Histopathological examination of the splenectomy specimen revealed multiple sickle cell clusters trapped within the microvasculature and confirmed diffuse splenic infarction

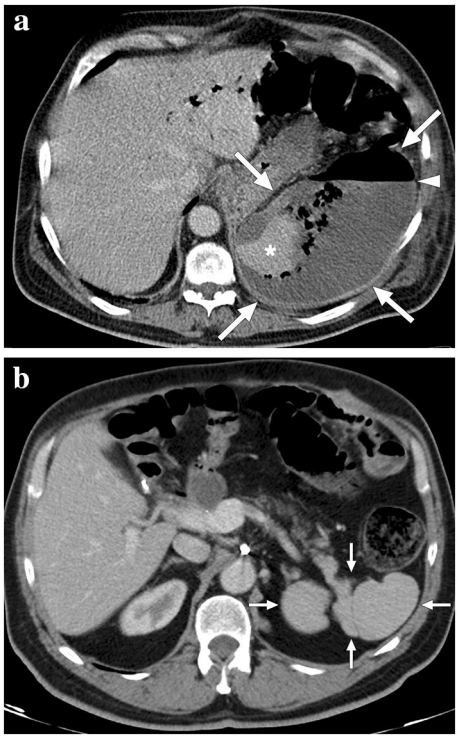

Fig. 23 A 60-year-old male patient with known pancreatic cancer. A splenic artery pseudoaneurysm and a large hematoma were detected in the surgical bed 10 days after the Whipple procedure, and endovascular embolization of the pseudoaneurysm was performed (not shown). The patient presented to ER with left upper quadrant pain, high fever, and chills 9 days after the embolization procedure. **a** Axial plane postcontrast abdominal CT showed a large splenic abscess with air–fluid level (arrowhead), which almost completely replaced the splenic parenchyma (arrows). Viable parenchyma could only be seen in a small area within the lower pole of the spleen (asterisk). Percutaneous abscess drainage revealed purulent content, and culture grew *Klebsiella pneumoniae*. The patient was placed on IV antibiotherapy after catheter placement and was discharged uneventfully within 3 weeks. **b** Follow-up abdominal CT 2 years after the initial presentation showed complete regression of splenic abscess and multilobulated residual spleen parenchymae (arrows)

hereditary thrombophilias may be associated with this clinical condition [57–59]. Adrenal infarcts related to systemic diseases are mostly bilateral, but unilateral infarcts may also be observed in a subset of patients [58]. The presence of a concomitant hemorrhage is important as non-hemorrhagic infarcts may be treated with anticoagulation, whereas a conservative approach is preferred in patients with hemorrhagic infarcts [59].

Early diagnosis is crucial for patients with bilateral AI as the clinical condition may suddenly deteriorate in certain patients due to hemodynamic collapse related to severe adrenal insufficiency. Furthermore, patients with unilateral involvement may suffer from sequential AI developing in the contralateral gland in a short interval, leading to an adrenal crisis [57].

As adrenal glands have a rich collateral arterial supply, they are relatively resistant to arterial ischemia. Therefore, AIs are mainly secondary to acute venous thrombosis and related parenchymal severe congestion/ischemia [57]. Arterial infarcts, however, may be seen due to extensive microarteriolar thrombi in certain patients, such as in cases with disseminated intravascular coagulation, DIC [57].

Despite the fact that the cause-effect relationship between hemorrhage and infarction is still controversial, it has been suggested that reperfusion injury secondary to the infarction may promote hemorrhage in certain cases [57].

CT and MRI are the most commonly utilized modalities for diagnosis. However, as gadolinium use may be limited in pregnant cases, CT may be preferred over MRI when there is a diagnostic need for an IV contrast study [58].

Non-enhancing and slightly thickened glands are the typical imaging findings in these patients. The so-called "capsular sign", which refers to the enhancing thin rim

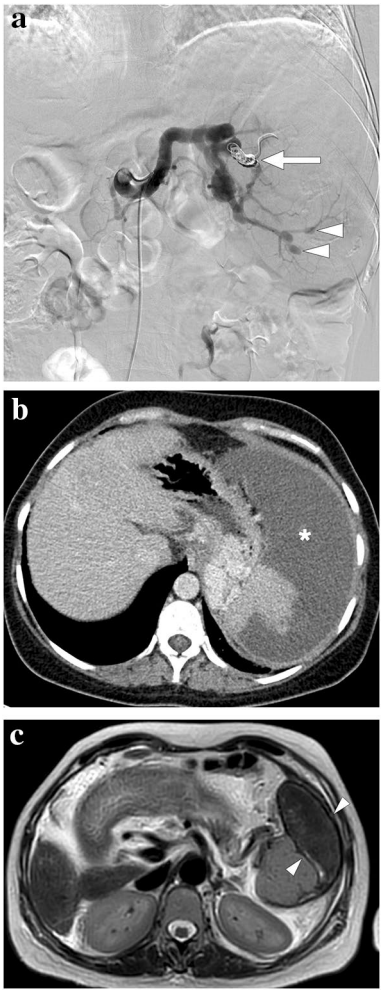

Fig. 24 A 39-year-old female patient with known cryptogenic cirrhosis, severe portal hypertension, and hypersplenism underwent partial splenic artery embolization. **a** Catheter angiography image shows the occluded upper pole branch of the splenic artery (arrow) with microparticle and coil embolization. Noted were multiple saccular aneurysms in the distal arterial branches of the lower pole (arrowheads). **b** Follow-up contrast-enhanced abdominal CT 6 weeks after the embolization shows large iatrogenic splenic infarction (asterisk). **c** Follow-up abdominal MR image 2 years after the embolization demonstrates the chronic phase of splenic infarct with a smaller size of the spleen and low T2 signal intensity within the regressed infarcted segment (arrowheads)

surrounding the nonenhancing adrenal parenchyma, may also be observed (Fig. 25) [59]. The hyperintense-looking adrenal gland on T2W images and accompanying diffusion restriction on DWI are typical findings on MRI in subjects with non-hemorrhagic infarcts [59]. However, it should be kept in mind that diffusion restriction is not specific to AI, and normal adrenal glands may also exhibit physiological diffusion restriction. On the other hand, the presence of asymmetric diffusion restriction compared to the contralateral adrenal gland may suggest infarction [60].

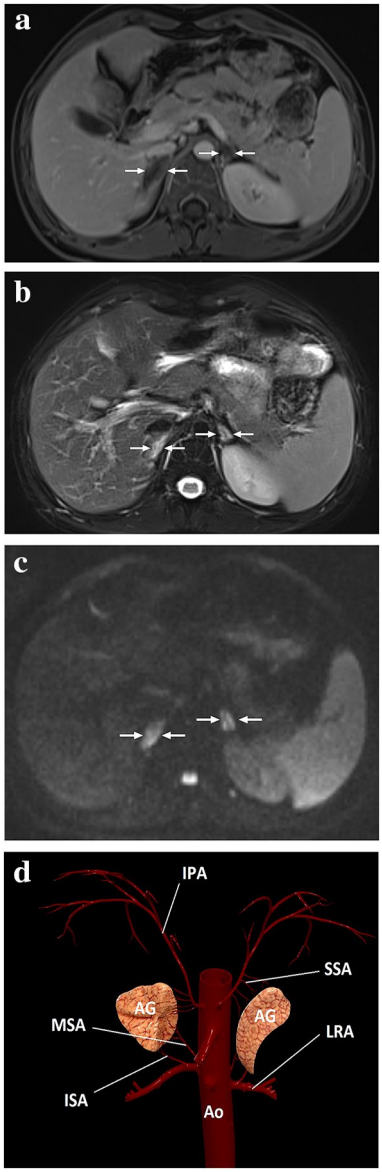

Fig. 25 A 20-year-old male patient with adrenal insufficiency due to antiphospholipid antibody syndrome. After bilateral mild adrenal hematomas had been detected on the initial abdominal CT, the patient was immediately placed on proper steroid replacement treatment, to which he quickly responded. **a** One week after the initial presentation, follow-up postcontrast abdominal MRI showed non-enhancing adrenal glands with a slight rim enhancement (arrows) and resolution of the adrenal hematomas. **b** Adrenal glands were significantly hyperintense on T2-weighted axial images (arrows). **c** On DWI images, both adrenal glands were diffusely hyperintense suggestive of restricted diffusion (arrows), which was also confirmed on the ADC map (not shown). The constellation of these imaging findings and his clinical symptoms was thought to represent bilateral adrenal infarction. Follow-up MRI obtained 2 years after the initial presentation showed bilateral glandular atrophy (not shown). **D** A 3D illustration shows the adrenal arterial supply. *IPA* inferior phrenic artery, *SSA* superior suprarenal arteries, *MSA* middle suprarenal artery, *ISA* inferior suprarenal arteries, *LRA* left renal artery, *AG* adrenal gland, *Ao* abdominal aorta

In the precontrast images, macroscopic hemorrhage in adrenal glands is typically observed as hyperdense on CT and hyperintense on T1W MR images, respectively (Fig. 26) [57]. In the subacute and chronic phases of hemorrhagic infarcts, MR signal characteristics tend to vary depending on the age of the blood products. It has been reported that adrenal pseudocysts, glandular atrophy, and calcifications may be seen in chronic phases of adrenal hemorrhages [61].

Adequate and detailed clinical history is crucial for correct diagnosis in these patients since rare cases of infectious (such as Waterhouse–Friderichsen syndrome), or drug-related adrenalitis may also mimic AIs on imaging (Fig. 27).

Intraperitoneal focal fat infarction

This entity refers to a self-limiting abdominal disease group characterized by focal acute inflammation and necrosis of intraabdominal adipose tissues, including acute omental infarcts (AOI), acute epiploic appendagitis (AEA), and acute perigastric appendagitis (APA).

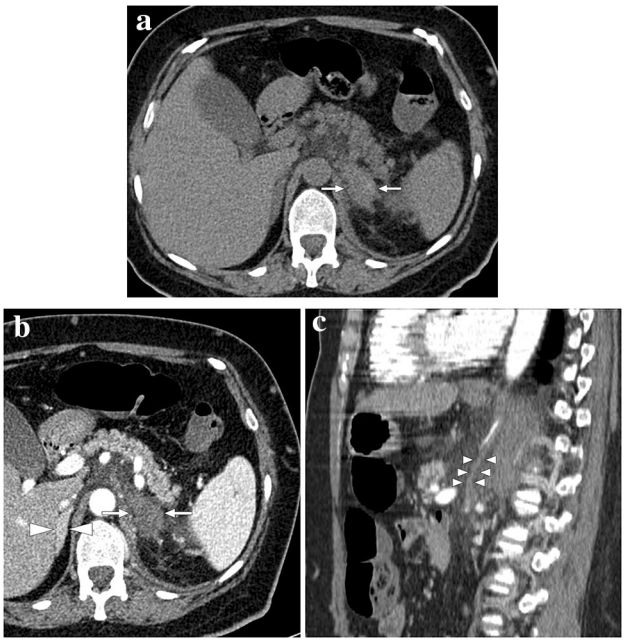

Fig. 26 A 47-year-old female with known long-standing antiphospholipid antibody syndrome and systemic lupus erythematosus presented with acute onset of intense left flank pain. **a** Axial plane precontrast abdominal CT showed enlarged, mostly hyperdense-appearing left adrenal gland (arrows). Also, note was made of striations within the adjacent fat planes. **b** There was no discernible enhancement within the adrenal gland after IV contrast injection (arrows). The right adrenal gland was normal (arrowheads). **c** Sagittal plane reformatted CT image of the same study demonstrated a vertically oriented, tubular structure that was thought to represent the thrombosed left adrenal vein (arrowheads). The constellation of imaging findings was found to be consistent with hemorrhagic adrenal infarction

Fig. 27 A 54-year-old female patient with metastatic non-small cell lung cancer who had been placed on immune checkpoint inhibitor (pembrolizumab) treatment. The patient acutely presented with abdominal pain and hypotension, suggesting an adrenal crisis. Adrenal insufficiency was confirmed on biochemical evaluation. Contrast-enhanced abdominal CT showed bilaterally enlarged and non-enhancing adrenal glands (arrowheads) with surrounding fat stranding. Clinical presentation and imaging findings were found to be suggestive of pembrolizumab-induced adrenalitis. The patient clinically responded well to steroid treatment. However, the patient expired due to widespread metastatic disease

Acute omental infarcts

AOIs are not among the common causes of acute abdominal pain. Pain in the right lower quadrant is a common clinical complaint with nausea, vomiting, anorexia, and fever [62]. The clinical and laboratory findings are nonspecific, and imaging plays a fundamental role in diagnosing and triaging patients. Acute cholecystitis and acute appendicitis are commonly confused clinical entities with AOI [63, 64]. Most cases are idiopathic with no detectable underlying cause, but several predisposing conditions such as accessory omentum, irregular omental fat accumulation, bifid omentum, and narrowed omental pedicle have been proposed. Heavy food intake, local trauma, rapid body movement, and coughing are other reported predisposing conditions [65].

CT is the most commonly used imaging modality for diagnosing AOI. The typical finding is a triangular-shaped, fat-containing heterogeneous mass between the abdominal wall and the transverse or ascending colon segments (Fig. 28) [66]. In the presence of a whirled pattern of linear strands, omental torsion may be considered as the cause of AOI [62]. Due to the close relationship between the colon and the increased adipose tissue density secondary to AOI, colonic diverticulitis may be confused with AOI. However, the absence of colonic diverticulosis, colonic wall thickening, and collection may favor AOI over colonic diverticulitis [67]. AEA is another important clinical entity that may mimic AOI. The size smaller than 5 cm, the presence of a surrounding hyperdense rim, and colonic wall abutment are other imaging features suggesting AEA over AOI [62, 68].

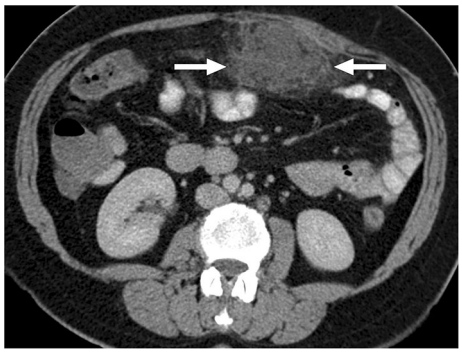

Fig. 28 A 56-year-old female patient presented to the ER with recent-onset, well-localized, severe periumbilical pain. Axial plane postcontrast abdominal CT image showed an intraabdominal heterogeneous fat-containing mass-like structure within the greater omentum (arrows). The imaging findings were considered to represent an omental infarct. The patient responded well to the supportive medical treatment, and a follow-up CT 1 month after the initial presentation revealed complete regression (not shown)

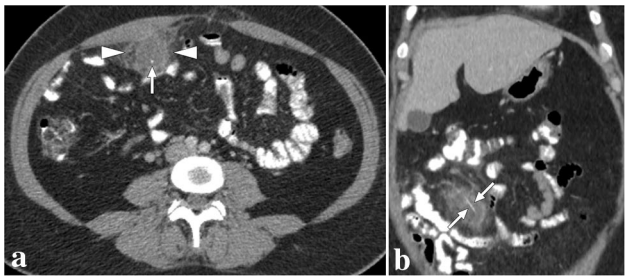

Fig. 29 A 43-year-old female presented with acute right-sided abdominal pain. **a** Axial plane postcontrast abdominal CT showed ill-defined mass-like omental lesion (arrowheads) with adjacent fat stranding. Note was also made of a hyperdense dot (arrow) within the lesion. Imaging findings were suggestive of an omental infarct, and the central hyperdense dot was thought to represent a thrombosed vascular structure, although it is an atypical finding for an omental infarct. The patient developed fever and progressively increasing abdominal pain despite maximum supportive treatment and finally underwent a laparoscopic excision to rule out secondarily infected omental infarct. Pathological evaluation revealed a nonneoplastic inflammatory omental mass containing a fishbone and foreign body reaction. **b** Based on pathological findings, a retrospective evaluation on the coronal plane demonstrated linear hyperdensity representing the fishbone (arrows)

Furthermore, focal inflammatory changes in the omentum secondary to various underlying conditions such as trauma, surgery, pancreatitis, and foreign body reaction may present with fat-containing pseudo mass appearance and mimic AOI (Fig. 29) [69].

Correct diagnosis is critical to prevent unnecessary surgical interventions because the treatment is primarily conservative. However, resection of the infarcted tissue may be needed when peritonitis signs worsen, or there is clinical suspicion of a complication [70, 71].

Acute epiploic appendagitis

AEA is a relatively rare cause of acute abdomen. Clinical diagnosis is mostly not possible, and imaging is, therefore, essential for diagnosis. Clinically, it is a benign, self-limiting disease, but the pain may be quite intense in the acute stage.

Anatomically, epiploic appendages (also called epiploicae appendices) are fatty outpouchings located on the colonic wall, and there are around 50–100 epiploic appendages in an adult colon [72, 73]. Epiploic appendages may be found near the appendix vermiformis and are absent in the rectum [74]. They are typically 2–5 cm in length with a thickness of 1–2 cm and tend to be larger in obese and in those who have recently lost weight [75, 76]. The vascular supply of the epiploic appendages is limited, and their increased mobility renders them susceptible to torsion and infarcts [74]. In primary AEA, the underlying pathophysiology is related to a torsed pedicle causing ischemic or hemorrhagic infarction with a thrombosed central vein. Among the secondary causes of AEA, inflammatory processes such as diverticulitis, pancreatitis, cholecystitis, or appendicitis may be counted [74]. In both conditions, the typical clinical symptomatology is characterized by focal, non-migrating abdominal pain in the left or right lower quadrants with no change in patient position. The treatment is mainly conservative, and surgery is almost never indicated. However, some authors have suggested that surgical removal represents the only way to avoid adhesion formation, recurrence, and intussusception induced by focal inflammation [77]. Areas adjacent to the sigmoid colon, the descending colon, and the right hemicolon, in decreasing order, are the most common sites of the disease [73]. As the clinical signs and symptoms are nonspecific, imaging, especially CT, plays a fundamental role in correct diagnosis.

The typical CT finding in patients with AEA is an oval fat-containing lesion with a diameter of less than 5 cm, surrounded by inflammation (Fig. 30) [78]. Intestinal obstruction and abscess formation are not expected. The local inflammation may also cause thickening of the adjacent parietal peritoneum and colonic wall (Fig. 31). The so-called "central dot sign", which refers to a thrombosed vein, is highly characteristic for diagnosis. However, its absence should not rule out the diagnosis [73]. Acute diverticulitis may simulate AEA on CT studies. However, a size smaller than 5 cm, the absence of extraluminal air and fluid, and abscess formation are helpful for differential diagnosis.

Acute perigastric appendagitis

APA is a rare entity characterized by ischemia and inflammation of the perigastric ligaments (falciform, gastrohepatic, gastrocolic, and gastrosplenic ligaments).

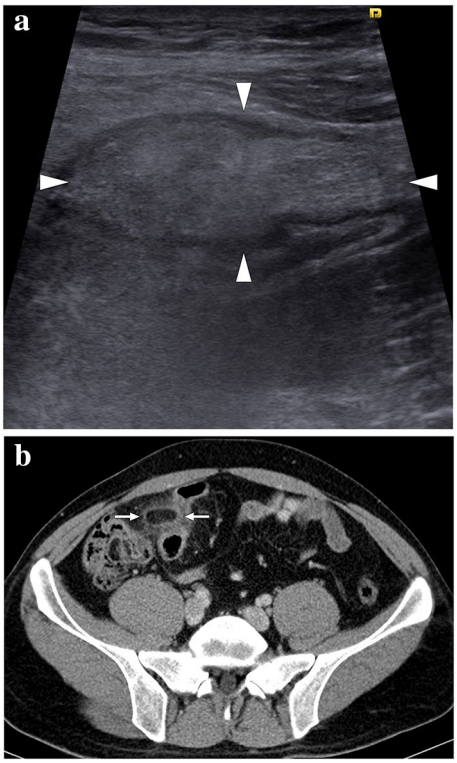

Fig. 30 A 23-year-old male patient presented with well-localized, severe right lower quadrant pain. **a** Grayscale US showed a non-compressible, oval-shaped, hyperechoic lesion (arrowheads) surrounded by a hypoechoic rim and increased echogenicity in the adjacent fat planes. **b** Axial plane postcontrast abdominal CT image demonstrated an ovoid lesion with internal fat density, peripheral high-density rim, and perilesional inflammatory stranding (arrows) adjacent to the sigmoid colon. Imaging findings were found to be compatible with epiploic appendagitis. The patient responded well to the supportive medical treatment

Fig. 31 A 29-year-old male patient presented with acute onset, severe left lower quadrant pain. Axial plane postcontrast abdominal CT showed an oval-shaped fatty lesion (arrows) in the left lower quadrant with peripheral inflammatory fat stranding, consistent with epiploic appendagitis. Note was also made of thickened adjacent parietal peritoneum secondary to the local inflammation (arrowheads). The patient responded well to the supportive medical treatment

Falciform ligament connects the liver to the anterior abdominal wall and contains the involuted umbilical vein remnant. It also has a connection with the lesser omentum [79]. Gastrohepatic ligament, a part of the lesser omentum, is also anatomically close to falciform ligament, and this anatomic structure connects the stomach to the liver. The remaining two perigastric ligaments are the gastrocolic and gastrosplenic ligaments, which are located between the transverse colon and the greater curvature of the stomach, and the spleen and the greater curve of the stomach, respectively.

All these perigastric ligaments have epiploic appendages, which may undergo torsion and subsequent infarct. Infarcts of these perigastric appendages appear to be extremely rare compared to colonic AEA, and there is not much information in the literature regarding their clinical and imaging aspects [79]. Accurate diagnosis is critical for ruling out more severe clinical mimickers and guiding treatment. For example, falciform ligament torsion may present with severe right hypochondrium pain or epigastric pain accompanied by elevated inflammatory markers. If it is not diagnosed radiologically, it may cause unnecessary interventions such as upper gastrointestinal endoscopy, laparoscopy, or laparotomy [80, 81]. As the clinical course of APA appears to be self-limiting and responsive to supportive non-invasive treatment, correct diagnosis with imaging gains even more importance.

CT is the workhorse in diagnosing acute abdominal pain. Therefore, most of the information on APA is based on this modality. The CT imaging characteristics of APA are not different from those of colonic AEA. Oval-shaped, heterogeneously appearing focus with associated surrounding stranding in the fat planes, consistent with edema, is the most typical imaging finding. The twisted infarcted fatty appendage can also be seen in falciform ligament torsion (Fig. 32) [80]. The rim around the torsed appendage is another relatively common finding (Fig. 33). The size of the abnormal area is also variable, with an average diameter of 4 cm. Mild adjacent gastric antral thickening has been reported in patients with gastrohepatic ligament appendagitis [79].

Ovarian torsion

Ovarian torsion (OT) is an uncommon cause of acute abdominal and pelvic pain. The cascade of events starts with the twisting of the ovarian pedicle and/or fallopian tubes. Concomitant torsion of the ovary and the tubes has been reported in 67% of cases of adnexal torsion [82, 83]. Unless surgical correction is performed timely, the subsequent vascular compromise leads to hemorrhagic infarction of the affected ovary [84]. Early diagnosis and treatment are mandatory since the delay of surgical intervention eventually

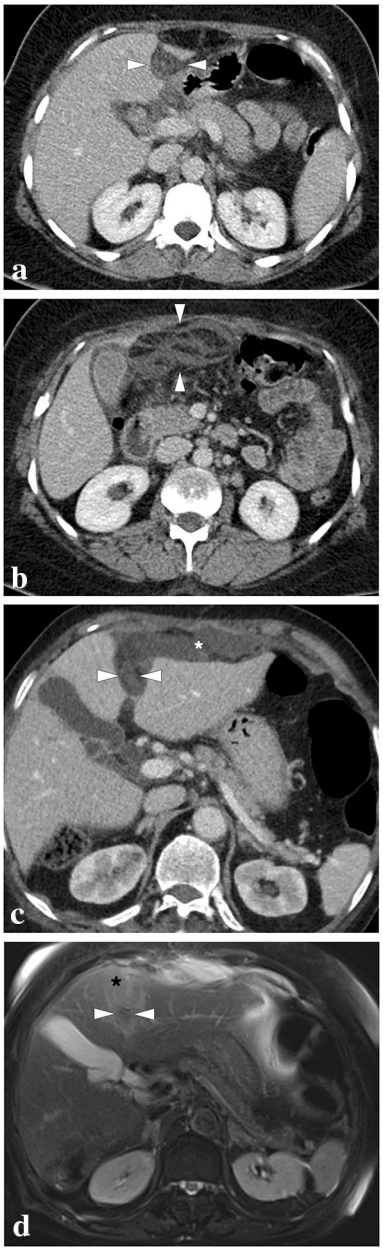

Fig. 32 Falciform ligament torsion in two different patients. **a** and **b** A 50-year-old female patient presented to ER with intense epigastric pain. **a** Axial plane postcontrast CT image showed thickened falciform ligament and periligamentous inflammatory stranding (arrowheads). **b** The inflammatory changes were seen to track downwards posterior to the anterior abdominal wall (arrowheads). Imaging findings were considered to represent falciform ligament torsion, and the patient's symptoms completely subsided with supportive medical treatment within a week. **c** and **d** An 86-year-old female patient presented with mild fever and recent-onset, severe epigastric pain. **c** Axial plane postcontrast CT image showed thickening of the ligamentum teres (arrowheads) with accompanying inflammatory stranding along the course of the falciform ligament extending anteriorly (asterisk). **d** Axial plane T2-weighted fat-suppressed MR image demonstrated the enlarged ligamentum teres (arrowheads) and surrounding inflammatory changes as increased T2 signal intensity (asterisk). Imaging findings were suggestive of falciform ligament torsion, and the patient responded well to the supportive medical treatment

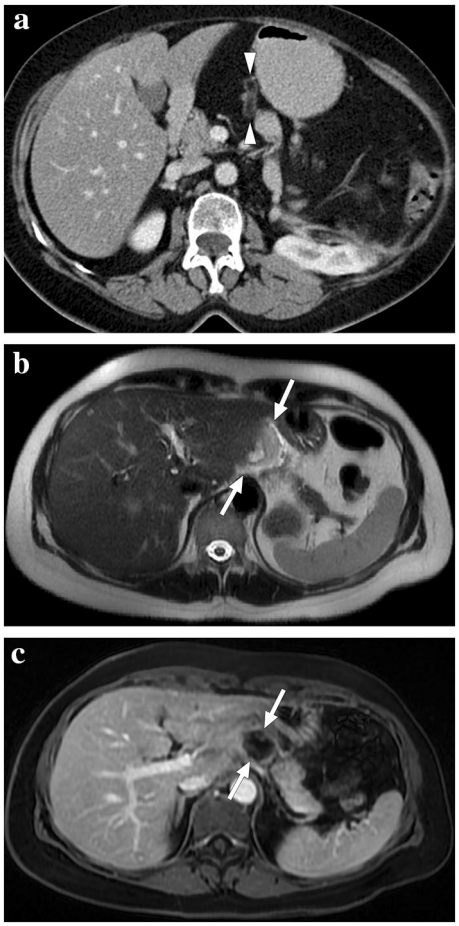

Fig. 33 Perigastric appendagitis in two different patients. **a** 62-year-old female presented with acute onset epigastric pain. Axial plane postcontrast abdominal CT showed an almost entirely fatty, tubular-shaped lesion with a hyperdense rim (arrowheads) in the gastrohepatic ligament. Findings were considered to represent perigastric appendagitis. Her pain completely subsided with supportive medical treatment. **b** and **c** A 54-year-old female presented with acute epigastric pain and a hyperechoic mass-like lesion adjacent to the left liver lobe on US (not shown). **b** Axial plane T2-weighted MR image revealed a mildly hyperintense mass-like lesion (arrows) in the gastrohepatic ligament with surrounding minimal free fluid. **c** Axial plane postcontrast MR image showed thin peripheral enhancement of this lesion with no apparent enhancement (arrows). Imaging findings were compatible with fat necrosis due to perigastric appendagitis. The patient was treated conservatively and fully recovered

leads to irreversible tissue loss. As the clinical findings are highly nonspecific, imaging plays a crucial role in the positive outcome of these patients.

US is almost always the first imaging modality used in female patients with acute pelvic pain as it is non-invasive, easily accessible, and cost-effective. An enlarged ovary is one of the most common imaging findings of OT on gray-scale US [82]. This enlargement may be detected even in the early phase of the disease before the development of infarction. On average, the organ volume may be up to 28 times

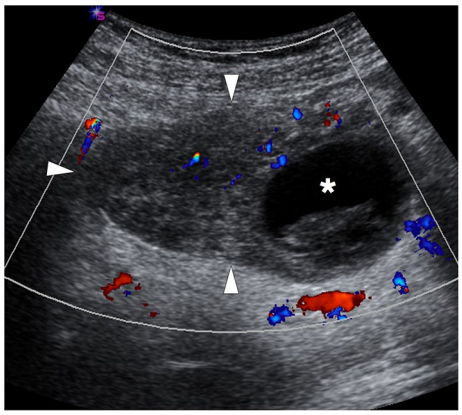

Fig. 34 A 33-year-old female patient presented with acute onset abdominal pain in the right lower quadrant. Color Doppler US showed an asymmetrically enlarged right ovary with heterogeneous stroma (arrowheads) and diminished-(but still preserved) parenchymal vascularity. Clinical and radiological findings were found to be consistent with ovarian torsion. Also, note was made of a peripherally located hemorrhagic cyst (asterisk), which was thought to be the culprit focus for the ovarian torsion. This ovary was surgically detorsed in emergency surgery

the normal size in torsed ovaries [85]. Heterogeneity of the ovarian stroma due to hemorrhage and edema is another important sonographic feature (Fig. 34). The presence of cysts within the ovarian stroma is a predisposing factor for OT, with benign mature cystic teratomas being the most common [86]. Peripherally displaced follicles, likely due to stromal edema and venous congestion, is another important diagnostic clue. Peripherally located cysts may also be seen in normal ovaries, but detecting these cysts in a unilaterally enlarged ovary is suggestive of OT [85].

Color Doppler imaging may also be beneficial as vascular compromise is the basis of ovarian ischemia/infarction in these patients. The absence of arterial flow on color Doppler imaging is a highly specific finding for OT; however, vice versa is not valid. Relying solely on the presence of parenchymal arterial flow can be quite deceiving to rule out OT, because the arterial flow signal is absent on imaging in only 73% of OT cases [82]. The diminished arterial flow is typically associated with venous flow abnormality [82].

Although not very common, CT is also used for diagnosing OT in certain patients. Although CT findings are not very specific, it is beneficial to rule out other clinical mimickers. The enlarged ovary displaced into the midline or the contralateral side, ascites, and peripherally displaced follicles may also be detected with CT. Other imaging findings include the absence of parenchymal enhancement, gas formation within the torsed mass, and obliteration of fat planes [87–89].

MRI offers unique benefits for evaluating the female pelvis due to its high soft-tissue resolution and lack of ionizing radiation. Its high resolution may obviate the need for IV contrast injection, which may benefit patients with limited renal reserve. Isolated ovarian and combined ovarian and adnexal torsion may be effectively evaluated with MRI. Ovarian edema and hemorrhage may be detected efficiently with MRI [90]. Peripherally displaced follicles, enlarged ovary, and heterogeneous stroma are all indicative for diagnosing OT. Alternative diagnoses may also be efficiently evaluated with MRI. The detection of T2 hypointense ovarian rim has also been suggested as an imaging indicator of OT (Fig. 35) [90].

In addition to those parenchymal changes, a twisted pedicle, a pathognomonic finding, can also be observed, especially on MRI and US [91].

The absence of parenchymal enhancement in postcontrast images may indicate a transition from ischemia to infarction [91]. However, the absence of abnormal ovarian enhancement on MRI does not entirely rule out the possibility of OT, like in Doppler US [91].

Clinical presentation and radiological findings may be confusing in partial or intermittent OT due to recurrent torsion/detorsion episodes [92]. Therefore, it is vital to consider

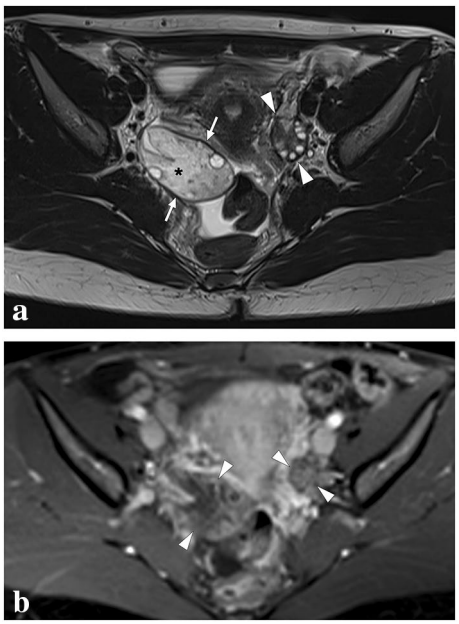

Fig. 35 A 30-year-old female patient presented to ER with acute-onset severe abdominal pain in the lower abdomen. US examination revealed an asymmetrically enlarged right ovary (not shown). **a** Axial plane T2-weighted MR image showed an asymmetrically enlarged right ovary (arrows) compared to its left counterpart (arrowheads). Diffuse stromal T2 hyperintensity due to parenchymal edema (asterisk), peripherally displaced ovarian follicles, T2 hypointense ovarian rim (arrows), and pelvic free fluid are other typical imaging findings for ovarian torsion. **b** Axial T1W fat-suppressed postcontrast image demonstrated diminished stromal contrast enhancement of the right ovary compared to the left one (arrows). Emergent surgical detorsion was performed immediately after this MR examination

the possibility of torsion in female patients presenting with acute pelvic pain, as early diagnosis and early intervention increase the likelihood of organ salvage.

Testicular ischemia and infarction

The testicular arteries originate from the abdominal aorta and pass through the inguinal canal to supply the testicular parenchyma. Testicular ischemia and infarcts usually present with acute scrotal pain and may require medical management or emergency surgical intervention depending on the cause. Although the most common causes of acute scrotal pain are epididymoorchitis, torsion of the appendix testis, and testicular torsion, it is important to keep in mind other rarer causes. US and Doppler US are indispensable tools for the differential diagnosis and management of these conditions presenting with similar symptoms.

In testicular torsion, decreased, absent, or abnormally high-resistance flow is expected in the symptomatic testis on Doppler US. While compromised venous drainage secondary to the torsion causes a high resistive index (> 0.75) in the early period, arterial occlusion in the advanced stage results in absent flow [93]. In addition, testicular enlargement, echotexture change, and spermatic cord twisting are other valuable radiological findings on gray scale US (Fig. 36). Early diagnosis (especially in the first 6 h) is critical for tissue viability. On the other hand, partial torsion can be confusing both clinically and radiologically due to spontaneous detorsions. After spontaneous detorsion, increased parenchymal vascularity mimicking orchitis can be observed on Doppler US [93].

Segmental testicular infarction (STI) is a rare and mostly idiopathic condition seen in patients aged 20–40. However, it is well-known that it may be seen secondary to vasculitis, trauma, hematological diseases, and infections [94, 95]. On scrotal US, STI is characterized by a wedge-shaped heterogeneous lesion with the apex pointing to the testicular mediastinum. Although the absence of flow on Doppler US helps distinguish STI from the mass, follow-up imaging may be required to exclude malignancy. MRI can be beneficial in cases where the differential diagnosis cannot be made with US. Non-enhancing, relatively well-defined heterogeneous parenchymal area peripherally outlined by capsular rim enhancement on postcontrast MR images suggests STI (Fig. 37). Additionally, hemorrhagic changes characterized by hyperintensities on T1 precontrast images can be seen within the infarct [94, 95].

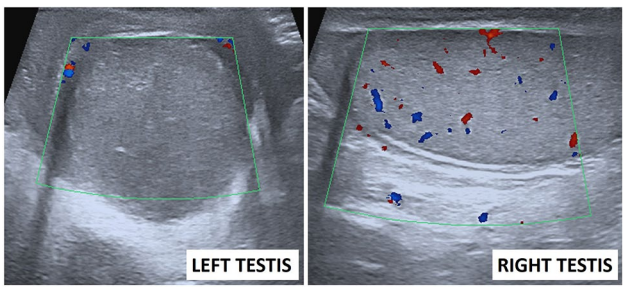

Fig. 36 A 28-year-old male presented to the ER with severe left testicular scrotal pain lasting approximately 12 h. On Color Doppler US images, the left testis is enlarged, has a hypoechoic appearance, and lacks parenchymal vascularity compared to the right testis. Imaging findings were consistent with left testicular torsion; an emergent surgery confirmed the diagnosis

Finally, it should be kept in mind that sequelae of testicular trauma, torsion or epididymoorchitis, extrinsic factors such as fluid collection, mass, inguinal hernia or hematoma compressing testicular parenchyma, and iatrogenic testicular artery injury (e.g., inguinal hernia repair) may cause testicular ischemia and may present with decreased/absent flow on Doppler US [93, 96].

Simultaneous multiple intraabdominal infarcts

In patients with multiple foci of parenchymal infarcts in different intraabdominal organs, various pro-thrombotic conditions should be considered as the underlying etiology [97]. Among the most common causes of multiple intraabdominal infarcts, hereditary thrombophilias, antiphospholipid antibody disease, Behcet's disease, and cardioembolic conditions (such as atrial fibrillation and infective endocarditis) may be considered initially (Fig. 38). Additionally, certain hematological diseases that may increase the tendency towards thrombus formation, such as DIC and heparin-induced thrombocytopenia, malignancy-associated coagulopathy (Trousseau syndrome), connective tissue diseases, vasculitides, and shock state should also be borne in mind (Fig. 39). Among the other rare causes, amniotic fluid embolism, fat/cholesterol crystal embolism, medication-induced thrombosis, and nephrotic syndrome may be counted.

More recently, with the onset of the global COVID-19 pandemic, multiple intraabdominal infarcts related to this infection have been observed and reported increasingly [98, 99]. It is now well-known that this infection may induce thromboembolic complications due to severe systemic inflammatory response, endothelial injury, and hypoxia (Fig. 40) [100].

In case of any extensive thromboembolism, infarction of several intraabdominal organs with extensive vascular supply and rich collateral circulation, such as the stomach, pancreas, and urinary bladder may be observed [101–105]. Despite mentioned infarct resistance of those organs, anecdotal case reports of infarcts have been reported in certain clinical conditions such as DIC and cholesterol crystal

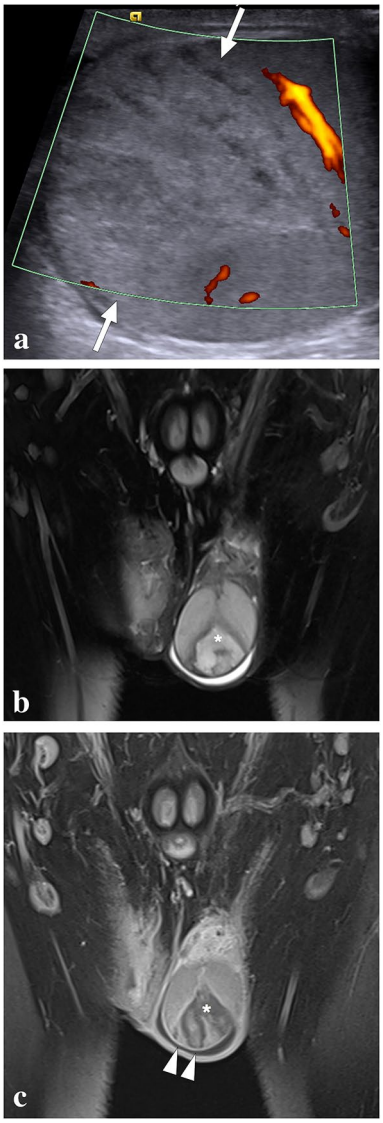

Fig. 37 A 32-year-old male with known Behcet's disease presented to the ER with acute scrotal pain. There was no history of trauma. **a** On power mode Doppler US, a triangular-shaped heterogeneous hyperechoic lesion with no apparent vascularity is seen (arrows). **b** Coronal T2W fat-suppressed MR image shows a triangular heterogeneous hyperintense lesion (asterisk) with the apex pointing towards the testicular mediastinum and surrounded by a T2 hypointense rim. Mild reactive hydrocele is also noted. **c** Coronal postcontrast T1W fat-suppressed MR image demonstrates the hypoenhancing lesion (asterisk) with sharp borders and peripheral rim enhancement (arrowheads). Imaging findings were consistent with segmental testicular infarction, likely related to Behcet's disease. The patient was placed on supportive treatment, to which he responded well

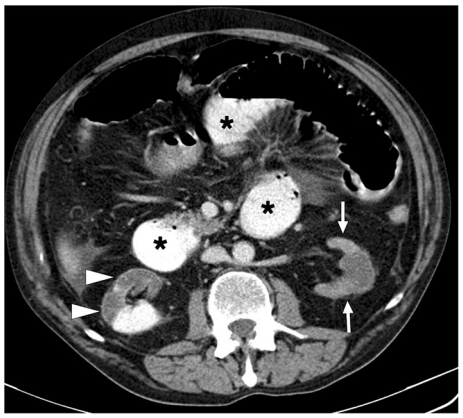

Fig. 38 A 59-year-old male patient with known congestive heart failure and atrial fibrillation presented with abdominal distention and diffuse abdominal pain to the ER. Axial plane postcontrast abdominal CT image showed a diffuse decrease in the parenchymal enhancement of the left kidney (arrows) and a large right renal infarct with thin cortical enhancement, so-called the cortical rim sign (arrowheads). Noted were dilated small bowel loops (asterisks), which were later surgically confirmed to be secondary to intestinal ischemia

Fig. 39 A 52-year-old female patient with known long-standing chronic renal failure on hemodialysis, multiple myeloma, and end-stage gastric adenocarcinoma recently underwent intense chemotherapy and now presented with high fever, severe abdominal pain, hypotension, and lethargy. Clinical examination revealed severe abdominal tenderness and mild jaundice. Laboratory studies revealed an abrupt increase in liver function tests. Findings were suggestive of septic shock, and blood cultures were also drawn. An emergent thoracoabdominal CT was performed to evaluate the potential source of infection. Axial plane postcontrast abdominal CT showed brisk enhancement in adrenal glands (arrowheads), suggesting severe metabolic stress. Also noted were extensive hypodense areas throughout the liver parenchyma (white asterisks), which were thought to represent parenchymal infarcts or perfusion defects. Also noted were globally infarcted spleen (black asterisk). The patient was immediately transferred to ICU; however, she expired 6 h after this CT scan. Blood cultures grew *Klebsiella pneumoniae*

embolism [101, 103]. As expected, it has been proposed that infarcts of these organs may develop as a result of massive microemboli to the distal vascular bed rather than a major arterial occlusion.

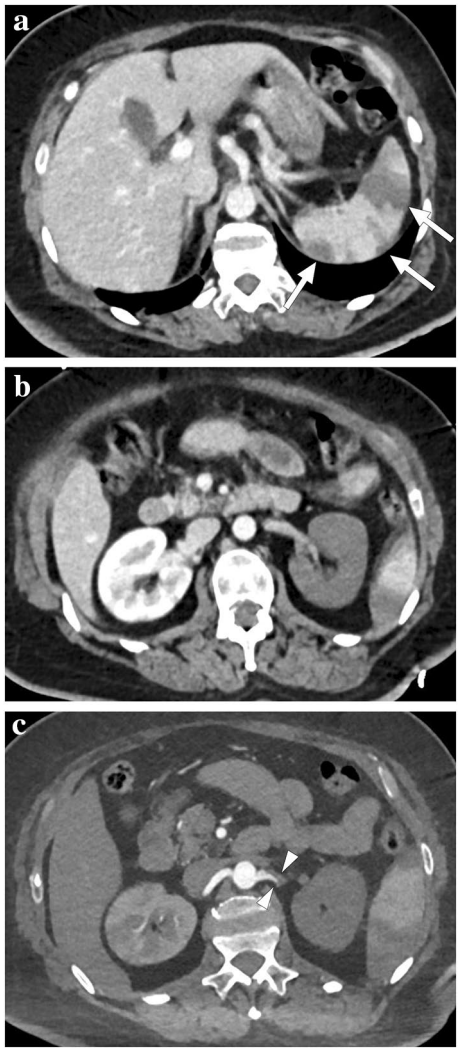

Fig. 40 A 57-year-old male patient with multiple comorbidities and severe COVID-19 infection necessitated intensive care unit admission. The patient expressed sudden-onset dyspnea and severe left upper quadrant pain during follow-up. **a**–**c** Contrast-enhanced thoracoabdominal CT revealed deep vein thrombosis (not shown), massive pulmonary thromboembolism (not shown), multiple splenic infarcts (arrows, **a**), global devascularization of the left kidney (**b**) secondary to the occlusion of the left renal artery (arrowheads, **c**), and small-sized, patchy right renal infarcts (not shown). Despite maximum supportive care, the patient continued to deteriorate, developed multiple embolic infarcts in the brain (not shown), and expired shortly afterward

Conclusion

The early detection of ischemia and infarcts in the abdomen is crucial for preventing potentially devastating complications related to these diseases. Prompt medical or surgical intervention is of fundamental importance to ensure a good outcome. Imaging specialists can play a crucial role in patient management by guiding clinicians in choosing the correct imaging modalities, optimizing imaging protocols, making a timely and accurate diagnosis, and highlighting possible differential diagnoses when appropriate.

Acknowledgements We thank Dr. M. Ruhi Onur for providing the cases of splenic torsion and acute splenic sequestration crisis.

Author contributions ADK, OO, and VK wrote the manuscript and collected data. MCK and VK designed illustrations. MK, DA, MNO, MCK, and PFH provided cases and edited the text. All of the authors read and approved the final manuscript.

Funding Not applicable.

Data availability Data sharing is not applicable to this article as no datasets were generated or analyzed during the current study.

Declarations

Conflict of interest The authors declare that they have no competing interests.

Ethical approval Not applicable.

Informed consent Not applicable.

Consent for publication Not applicable.

References

1. Dhatt HS, Behr SC, Miracle A, Wang ZJ, Yeh BM. Radiological evaluation of bowel ischemia. Radiologic Clinics. 2015;53(6):1241–54.
2. Lourenco PD, Rawski R, Mohammed MF, Khosa F, Nicolaou S, McLaughlin P. Dual-energy CT iodine mapping and 40-keV monoenergetic applications in the diagnosis of acute bowel ischemia. American Journal of Roentgenology. 2018;211(3):564–70.
3. Obmann MM, Punjabi G, Obmann VC, Boll DT, Heye T, Benz MR, et al. Dual-energy CT of acute bowel ischemia. Abdominal Radiology. 2022;47(5):1660–83.
4. Virmani V, Ramanathan S, Virmani VS, Kielar A, Sheikh A, Ryan J. Non-neoplastic hepatic vascular diseases: spectrum of CT and MRI appearances. Clin Radiol. 2014;69(5):538–48.
5. Chen V, Hamilton J, Qizilbash A. Hepatic infarction. A clinicopathologic study of seven cases. Arch Pathol Lab Med. 1976;100(1):32–6.
6. Chuang CH, Chen CY, Tsai HM. Hepatic infarction and hepatic artery pseudoaneurysm with peritoneal bleeding after radiofrequency ablation for hepatoma. Clin Gastroenterol Hepatol. 2005;3(11):A23.
7. Cohen SE, Safadi R, Verstandig A, Eid A, Sasson T, Symmer L, et al. Liver-spleen infarcts following transcatheter chemoembolization: a case report and review of the literature on adverse effects. Dig Dis Sci. 1997;42(5):938–43.
8. Lopera JE, Katabathina V, Bosworth B, Garg D, Kroma G, Garza-Berlanga A, et al. Segmental liver ischemia/infarction after elective transjugular intrahepatic portosystemic shunt creation: clinical outcomes in 10 patients. J Vasc Interv Radiol. 2015;26(6):835–41.
9. Tzakis AG, Gordon RD, Shaw BW, Jr., Iwatsuki S, Starzl TE. Clinical presentation of hepatic artery thrombosis after liver transplantation in the cyclosporine era. Transplantation. 1985;40(6):667–71.

10. Bandyopadhyay S, Bandyopadhyay D. Acute Budd–Chiari syndrome as an initial presentation of acute promyelocytic leukemia. J Cancer Res Ther. 2010;6(4):567–9.
11. Boll DT, Merkle EM. Diffuse liver disease: strategies for hepatic CT and MR imaging. Radiographics. 2009;29(6):1591–614.
12. Stewart BG, Gervais DA, O'Neill MJ, Boland GW, Hahn PF, Mueller PR. Imaging and percutaneous treatment of secondarily infected hepatic infarctions. American Journal of Roentgenology. 2008;190(3):601–7.
13. Giovine S, Pinto A, Crispano S, Lassandro F, Romano L. Retrospective study of 23 cases of hepatic infarction: CT findings and pathological correlations. Radiol Med. 2006;111(1):11–21.
14. Smith GS, Birnbaum BA, Jacobs JE. Hepatic infarction secondary to arterial insufficiency in native livers: CT findings in 10 patients. Radiology. 1998;208(1):223–9.
15. Zimmermann A. Tumor-like necroses of the liver: liver infarct and hepatic pseudo-infarct (Zahn's infarct). Tumors and tumor-like lesions of the hepatobiliary tract Springer International Publishing Switzerland. 2017:2445–53.
16. Yim NY, Jeong YY, Shin SS, Song SG, Lim HS, Heo SH, et al. Hepatic perfusion disorders: a pictorial review of CT and MR imaging. Journal of the Korean Radiological Society. 2005;53(3):199–213.
17. Torabi M, Hosseinzadeh K, Federle MP. CT of nonneoplastic hepatic vascular and perfusion disorders. Radiographics. 2008;28(7):1967–82.
18. Brancatelli G, Vilgrain V, Federle MP, Hakime A, Lagalla R, Iannaccone R, et al. Budd–Chiari syndrome: spectrum of imaging findings. American Journal of Roentgenology. 2007;188(2):W168–W76.
19. Cura M, Haskal Z, Lopera J. Diagnostic and interventional radiology for Budd–Chiari syndrome. Radiographics. 2009;29(3):669–81.
20. Itai Y, Murata S, Kurosaki Y. Straight border sign of the liver: spectrum of CT appearances and causes. Radiographics. 1995;15(5):1089–102.
21. Deltenre P, Valla D-C. Ischemic cholangiopathy. Journal of Hepatology. 2006;44(4):806–17.
22. Kharmach O, Borahma M, Lagdali N, Benelbarhdadi I, Ajana F-Z. Ischemic cholangitis during Osler–Weber–Rendu disease: a case report. Egyptian Liver Journal. 2022;12(1):10.
23. Alabdulghani F, Healy G, Cantwell C. Radiological findings in ischaemic cholangiopathy. Clinical Radiology. 2020;75(3):161–8.
24. Hawthorn BR, Ratnam LA. Acute mesenteric ischaemia: imaging and intervention. Clin Radiol. 2020;75(5):398.e19–e28.
25. Klar E, Rahmanian PB, Bucker A, Hauenstein K, Jauch KW, Luther B. Acute mesenteric ischemia: a vascular emergency. Dtsch Arztebl Int. 2012;109(14):249–56.
26. Haga Y, Odo M, Homma M, Komiya K, Takeda K, Koike S, et al. New prediction rule for mortality in acute mesenteric ischemia. Digestion. 2009;80(2):104–11.
27. Wadman M, Syk I, Elmstahl S. Survival after operations for ischaemic bowel disease. Eur J Surg. 2000;166(11):872–7.
28. Oldenburg WA, Lau LL, Rodenberg TJ, Edmonds HJ, Burger CD. Acute mesenteric ischemia: a clinical review. Arch Intern Med. 2004;164(10):1054–62.
29. Bala M, Kashuk J, Moore EE, Kluger Y, Biffl W, Gomes CA, et al. Acute mesenteric ischemia: guidelines of the World Society of Emergency Surgery. World Journal of Emergency Surgery. 2017;12(1):1–11.
30. Trompeter M, Brazda T, Remy CT, Vestring T, Reimer P. Non-occlusive mesenteric ischemia: etiology, diagnosis, and interventional therapy. Eur Radiol. 2002;12(5):1179–87.
31. Chiu CJ, McArdle AH, Brown R, Scott HJ, Gurd FN. Intestinal mucosal lesion in low-flow states. I. A morphological, hemodynamic, and metabolic reappraisal. Arch Surg. 1970;101(4):478–83.
32. Fernandes T, Oliveira MI, Castro R, Araújo B, Viamonte B, Cunha R. Bowel wall thickening at CT: simplifying the diagnosis. Insights into imaging. 2014;5(2):195–208.
33. Arthurs ZM, Titus J, Bannazadeh M, Eagleton MJ, Srivastava S, Sarac TP, et al. A comparison of endovascular revascularization with traditional therapy for the treatment of acute mesenteric ischemia. J Vasc Surg. 2011;53(3):698–704; discussion -5.
34. Suzer O, Shirkhoda A, Jafri SZ, Madrazo BL, Bis KG, Mastromatteo JF. CT features of renal infarction. Eur J Radiol. 2002;44(1):59–64.
35. Antopolsky M, Simanovsky N, Stalnikowicz R, Salameh S, Hiller N. Renal infarction in the ED: 10-year experience and review of the literature. Am J Emerg Med. 2012;30(7):1055–60.
36. Harris AC, Zwirewich CV, Lyburn ID, Torreggiani WC, Marchinkow LO. Ct findings in blunt renal trauma. Radiographics. 2001;21 Spec No: S201-14.
37. Ambesh P, Lal H. Renal cortical rim sign. Abdominal imaging. 2015;40:2914–5.
38. Piccoli GB, Priola AM, Vigotti FN, Guzzo G, Veltri A. Renal infarction versus pyelonephritis in a woman presenting with fever and flank pain. American Journal of Kidney Diseases. 2014;64(2):311–4.
39. Kawashima A, Sandler CM, Corl FM, West OC, Tamm EP, Fishman EK, et al. Imaging of renal trauma: a comprehensive review. Radiographics. 2001;21(3):557–74.
40. Sugi MD, Joshi G, Maddu KK, Dahiya N, Menias CO. Imaging of renal transplant complications throughout the life of the allograft: comprehensive multimodality review. Radiographics. 2019;39(5):1327–55.
41. Spiesecke P, Munch F, Fischer T, Hamm B, Lerchbaumer MH. Multiparametric ultrasound findings in acute kidney failure due to rare renal cortical necrosis. Sci Rep. 2021;11(1):2060.
42. Prakash J, Vohra R, Wani IA, Murthy AS, Srivastva PK, Tripathi K, et al. Decreasing incidence of renal cortical necrosis in patients with acute renal failure in developing countries: a single-centre experience of 22 years from Eastern India. Nephrol Dial Transplant. 2007;22(4):1213–7.
43. Chen F, Alexander L, Caserta M. Reverse rim sign on CEUS. Abdom Radiol (NY). 2020;45(1):255–6.
44. Dyer RB, Chen MY, Zagoria RJ. Classic signs in uroradiology. Radiographics. 2004;24 Suppl 1:S247–80.
45. Regine G, Stasolla A, Miele V. Multidetector computed tomography of the renal arteries in vascular emergencies. Eur J Radiol. 2007;64(1):83–91.
46. Alabousi A, Patlas MN, Scaglione M, Romano L, Soto JA. Cross-sectional imaging of nontraumatic emergencies of the spleen. Curr Probl Diagn Radiol. 2014;43(5):254–67.
47. Unal E, Onur MR, Akpinar E, Ahmadov J, Karcaaltincaba M, Ozmen MN, et al. Imaging findings of splenic emergencies: a pictorial review. Insights into imaging. 2016;7(2):215–22.
48. Emery KH. Splenic emergencies. Radiol Clin North Am. 1997;35(4):831–43.
49. Paterson A, Frush DP, Donnelly LF, Foss JN, O'Hara SM, Bisset GS, III. A pattern-oriented approach to splenic imaging in infants and children. Radiographics. 1999;19(6):1465–85.
50. Antopolsky M, Hiller N, Salameh S, Goldshtein B, Stalnikowicz R. Splenic infarction: 10 years of experience. Am J Emerg Med. 2009;27(3):262–5.
51. Taylor AJ, Dodds WJ, Erickson SJ, Stewart ET. CT of acquired abnormalities of the spleen. AJR Am J Roentgenol. 1991;157(6):1213–9.
52. Levin TL, Berdon WE, Haller JO, Ruzal-Shapiro C, Hurlet-Jenson A. Intrasplenic masses of "preserved" functioning splenic tissue in sickle cell disease: correlation of imaging findings (CT,

ultrasound, MRI, and nuclear scintigraphy). Pediatr Radiol. 1996;26(9):646–9.
53. Feola A, Niola M, Conti A, Delbon P, Graziano V, Paternoster M, et al. Iatrogenic splenic injury: review of the literature and medico-legal issues. Open Medicine. 2016;11(1):307–15.
54. Kartha A, Sulaiman TO. Iatrogenic splenic infarction after embolization of an anomalous artery supplying a pulmonary sequestration: A report of a rare case. Yemen Journal of Medicine. 2022:97–9.
55. Ekeh AP, McCarthy MC, Woods RJ, Haley E. Complications arising from splenic embolization after blunt splenic trauma. The American Journal of Surgery. 2005;189(3):335–9.
56. Hadduck TA, McWilliams JP. Partial splenic artery embolization in cirrhotic patients. World J Radiol. 2014;6(5):160–8.
57. Riddell A, Khalili K. Sequential adrenal infarction without MRI-detectable hemorrhage in primary antiphospholipid–antibody syndrome. American Journal of Roentgenology. 2004;183(1):220–2.
58. Green P-AD, Ngai IM, Lee TT, Garry DJ. Unilateral adrenal infarction in pregnancy. Case Reports. 2013;2013:bcr2013009997.
59. Glomski SA, Guenette JP, Landman W, Tatli S. Acute nonhemorrhagic adrenal infarction in pregnancy: 10-year MRI incidence and patient outcomes at a single institution. American Journal of Roentgenology. 2018;210(4):785–91.
60. Padilla RM, Way AR, Soule E, Gopireddy D, Lall C. Diffusion Weighted Imaging in Unilateral Adrenal Infarction: A Case of Colicky Right Upper Quadrant Pain in a Pregnant Female. Cureus. 2021;13(2).
61. Jordan E, Poder L, Courtier J, Sai V, Jung A, Coakley FV. Imaging of nontraumatic adrenal hemorrhage. American Journal of Roentgenology. 2012;199(1):W91–W8.
62. Singh AK, Gervais DA, Lee P, Westra S, Hahn PF, Novelline RA, et al. Omental infarct: CT imaging features. Abdom Imaging. 2006;31(5):549–54.
63. Miguel Perello J, Aguayo Albasini JL, Soria Aledo V, Aguilar Jimenez J, Flores Pastor B, Candel Arenas MF, et al. [Omental torsion: imaging techniques can prevent unnecessary surgical interventions]. Gastroenterol Hepatol. 2002;25(8):493–6.
64. Puylaert JB. Right-sided segmental infarction of the omentum: clinical, US, and CT findings. Radiology. 1992;185(1):169–72.
65. Occhionorelli S, Zese M, Cappellari L, Stano R, Vasquez G. Acute Abdomen due to Primary Omental Torsion and Infarction. Case Rep Surg. 2014;2014:208382.
66. Hollerweger A, Rettenbacher T, Macheiner P, Gritzmann N. [Spontaneous fatty tissue necrosis of the omentum majus and epiploic appendices: clinical, ultrasonic and CT findings]. Rofo. 1996;165(6):529–34.
67. Garant M, Taourel P, Fried GM, Bret PM. Thickening of the transverse colon associated with torsion of the greater omentum. AJR Am J Roentgenol. 1995;165(5):1309.
68. Singh AK, Alhilali LM, Gervais DA, Mueller PR. Omental infarct: an unusual CT appearance after superior mesenteric artery occlusion. Emerg Radiol. 2004;10(5):276–8.
69. Nee C-H, Huang C-W, Chou S-C. Omental inflammatory mass secondary to a migrating fish bone: A case report. 中華民國急救加護醫學會雜誌. 2011;22(1):40–8.
70. Helmrath MA, Dorfman SR, Minifee PK, Bloss RS, Brandt ML, DeBakey ME. Right lower quadrant pain in children caused by omental infarction. Am J Surg. 2001;182(6):729–32.
71. Kimber CP, Westmore P, Hutson JM, Kelly JH. Primary omental torsion in children. J Paediatr Child Health. 1996;32(1):22–4.
72. Almeida AT, Melao L, Viamonte B, Cunha R, Pereira JM. Epiploic appendagitis: an entity frequently unknown to clinicians—diagnostic imaging, pitfalls, and look-alikes. AJR Am J Roentgenol. 2009;193(5):1243–51.
73. Singh AK, Gervais DA, Hahn PF, Sagar P, Mueller PR, Novelline RA. Acute epiploic appendagitis and its mimics. Radiographics. 2005;25(6):1521–34.
74. Giambelluca D, Cannella R, Caruana G, Salvaggio L, Grassedonio E, Galia M, et al. CT imaging findings of epiploic appendagitis: an unusual cause of abdominal pain. Insights Imaging. 2019;10(1):26.
75. Ghahremani GG, White EM, Hoff FL, Gore RM, Miller JW, Christ ML. Appendices epiploicae of the colon: radiologic and pathologic features. Radiographics. 1992;12(1):59–77.
76. Pereira JM, Sirlin CB, Pinto PS, Jeffrey RB, Stella DL, Casola G. Disproportionate fat stranding: a helpful CT sign in patients with acute abdominal pain. Radiographics. 2004;24(3):703–15.
77. Saad J, Mustafa HA, Elsani AM, Alharbi F, Alghamdi S. Primary epiploic appendagitis: reconciling CT and clinical challenges. Indian J Gastroenterol. 2014;33(5):420–6.
78. Singh AK, Gervais DA, Hahn PF, Rhea J, Mueller PR. CT appearance of acute appendagitis. AJR Am J Roentgenol. 2004;183(5):1303–7.
79. Justaniah AI, Scholz FJ, Katz DS, Scheirey CD. Perigastric appendagitis: CT and clinical features in eight patients. Clin Radiol. 2014;69(12):e531–7.
80. Maccallum C, Eaton S, Chubb D, Franzi S. Torsion of fatty appendage of falciform ligament: acute abdomen in a child. Case Reports in Radiology. 2015;2015.
81. O'Connor A, Sabri S, Solkar M, Ramzan A, Solkar M. Falciform ligament torsion as a rare aetiology of the acute abdomen. Journal of Surgical Case Reports. 2022;2022(1):rjab150.
82. Albayram F, Hamper UM. Ovarian and adnexal torsion: spectrum of sonographic findings with pathologic correlation. J Ultrasound Med. 2001;20(10):1083–9.
83. Breech LL, Hillard PJ. Adnexal torsion in pediatric and adolescent girls. Curr Opin Obstet Gynecol. 2005;17(5):483–9.
84. Duigenan S, Oliva E, Lee SI. Ovarian torsion: diagnostic features on CT and MRI with pathologic correlation. AJR Am J Roentgenol. 2012;198(2):W122–31.
85. Graif M, Shalev J, Strauss S, Engelberg S, Mashiach S, Itzchak Y. Torsion of the ovary: sonographic features. AJR Am J Roentgenol. 1984;143(6):1331–4.
86. Stark JE, Siegel MJ. Ovarian torsion in prepubertal and pubertal girls: sonographic findings. AJR Am J Roentgenol. 1994;163(6):1479–82.
87. Bennett GL, Slywotzky CM, Giovanniello G. Gynecologic causes of acute pelvic pain: spectrum of CT findings. Radiographics. 2002;22(4):785–801.
88. Kawahara Y, Fukuda T, Futagawa S, Sakamoto I, Takao M, Kinoshita Y, et al. Intravascular gas within an ovarian tumor: a CT sign of ovarian torsion. J Comput Assist Tomogr. 1996;20(1):154–6.
89. Rha SE, Byun JY, Jung SE, Jung JI, Choi BG, Kim BS, et al. CT and MR imaging features of adnexal torsion. Radiographics. 2002;22(2):283–94.
90. Petkovska I, Duke E, Martin DR, Irani Z, Geffre CP, Cragun JM, et al. MRI of ovarian torsion: Correlation of imaging features with the presence of perifollicular hemorrhage and ovarian viability. Eur J Radiol. 2016;85(11):2064–71.
91. Duigenan S, Oliva E, Lee SI. Ovarian torsion: diagnostic features on CT and MRI with pathologic correlation. American Journal of Roentgenology. 2012;198(2):W122–W31.
92. Chang HC, Bhatt S, Dogra VS. Pearls and pitfalls in diagnosis of ovarian torsion. Radiographics. 2008;28(5):1355–68.
93. Alexander LF, Caserta MP, Baden K, Livingston D, Cernigliaro JG, Bhatt S. Absent, abnormal, or reduced flow in the testis: thinking beyond torsion. RadioGraphics. 2020;40(2):529–30.

94. Cassidy FH, Ishioka KM, McMahon CJ, Chu P, Sakamoto K, Lee KS, et al. MR imaging of scrotal tumors and pseudotumors. Radiographics. 2010;30(3):665–83.
95. Fernández-Pérez GC, Tardáguila FM, Velasco M, Rivas C, Dos Santos J, Cambronero J, et al. Radiologic findings of segmental testicular infarction. American Journal of Roentgenology. 2005;184(5):1587–93.
96. Dellabianca C, Bonardi M, Alessi S. Testicular ischemia after inguinal hernia repair. Journal of Ultrasound. 2011;14(4):205–7.
97. Olson MC, Lubner MG, Menias CO, Mellnick VM, Mankowski Gettle L, Kim DH, et al. Venous thrombosis and hypercoagulability in the abdomen and pelvis: causes and imaging findings. RadioGraphics. 2020:190097.
98. Bhayana R, Som A, Li MD, Carey DE, Anderson MA, Blake MA, et al. Abdominal imaging findings in COVID-19: preliminary observations. Radiology. 2020;297(1):E207–E15.
99. Besutti G, Bonacini R, Iotti V, Marini G, Riva N, Dolci G, et al. Abdominal visceral infarction in 3 patients with COVID-19. Emerging Infectious Diseases. 2020;26(8):1926.
100. Mondal S, Quintili AL, Karamchandani K, Bose S. Thromboembolic disease in COVID-19 patients: a brief narrative review. Journal of Intensive Care. 2020;8(1):1–10.
101. Harvey RL, Doberneck RC, Black III WC. Infarction of the stomach following atheromatous embolization: report of a case and literature review. Gastroenterology. 1972;62(3):469–72.
102. Cohen EB. Infarction of the stomach: report of three cases of total gastric infarction and one case of partial infarction. The American Journal of Medicine. 1951;11(5):645–52.
103. Park DH, Kwon T-H, Cho HD, Park JH, Lee S-H, Park S-H, et al. Pancreatic infarction resulting from cholesterol crystal embolism mimicking a solid pancreatic tumor. Gastrointestinal Endoscopy. 2008;67(1):176–8.
104. Matsukuma S, Suda K. Pancreatic Ischemic Lesions. Pancreas-Pathological Practice and Research: Karger Publishers; 2007. p. 36–44.
105. Nino-Murcia M, Friedland GW. Bladder infarct. Urologic Radiology. 1988;9(1):234–6.

Authors and Affiliations

Ali Devrim Karaosmanoglu[1] · Omer Onder[1] · Volkan Kizilgoz[2] · Peter F. Hahn[3] · Mecit Kantarci[2,4] · Mustafa Nasuh Ozmen[1] · Musturay Karcaaltincaba[1] · Deniz Akata[1]

[1] Department of Radiology, Hacettepe University School of Medicine, 06100 Ankara, Turkey

[2] Department of Radiology, Erzincan Binali Yıldırım University School of Medicine, 24100 Erzincan, Turkey

[3] Department of Radiology, Massachusetts General Hospital, Harvard Medical School, Boston, MA 02114, USA

[4] Department of Radiology, Atatürk University School of Medicine, 25240 Erzurum, Turkey